Peer-reviewed version available at Remote Sens. 2018, 10, 1397; doi:10.3390/rs10091397

Article

UAV remote sensing for biodiversity monitoring: are forest canopy gaps good covariates?

Martin B. Bagaram [1*], Diego Giuliarelli [2], Gherardo Chirici [3], Francesca Giannetti [3], Anna Barbati[2]

1. School of Environment and Forest Science, University of Washington, Box 352100, Seattle, WA 98195, USA. Email: martb@uw.edu,
2. Department for Innovation in Biological, Agro-Food and Forest System, Università degli Studi della Tuscia, Viterbo, Italy. Email: dgiuliarelli@unitus.it (DG); barbati.sisfor@unitus.it (AB)
3. Department of Agricultural, Food and Forestry System, Università degli Studi di Firenze, Via San Bonaventura, Florence, Italy; Email: gherardo.chirici@unifi.it (GC); francesca.giannetti@unifi.it (FG)

* Correspondence: martb@uw.edu; Tel: +12064809334 (MB)

Abstract: Forest canopy gaps are important for the ecosystem dynamics. Depending on tree species, small canopy openings might be also associated to intra-crown porosity and to space between crowns. Yet, little is known on the relationships between the fine-scaled pattern of canopy openings and biodiversity features. This research explored the possibility of i)- mapping forest canopy gaps from a very high resolution orthomosaic (10 cm), processed from a versatile imaging platform such as unmanned aerial vehicles (UAV), ii)- to derive patch metrics that can be tested as covariates of variables of interest for forest biodiversity monitoring. This is attempted in a test area of 240 ha covered by temperate deciduous forest types in Central Italy and containing 50 forest inventory plots of about 530 m^2. Correlation and linear regression techniques were used to explore relationships between patch metrics and understorey (density, development and species diversity) or forest habitat biodiversity variables (density of micro-habitat bearing trees, vertical species profile, tree species diversity). The results revealed that small openings in the canopy cover (75% smaller than 7 m^2) can be faithfully extracted from UAV RGB imagery, using the red band and contrast split segmentation. Highest correlations were observed in the mixed forest (beech and turkey oak), while beech forest had the poorest ones and turkey oak forest displayed intermediate results. Moderate to strong linear relationships were found between gap metrics and understorey variables in mixed forest type, with adjusted R^2 from linear regression ranging from 0.52 to 0.87. Equally good results, in the same forest types, were observed for forest habitat biodiversity variables ($0.52<\text{adjusted } R^2<0.79$) with highest values found for density of trees with microhabitats and vertical species profile. In conclusion, this research highlights that UAV remote sensing can potentially provide covariate surfaces of variables of interest for forest biodiversity monitoring, conventionally collected in forest inventory plots. By integrating the two sources of data, these variables can be mapped over small forest areas with satisfactory levels of accuracy, at a much higher spatial resolution than would be possible by field-based forest inventory solely.

Keywords: Unmanned Aerial systems (UAS), RGB high resolution imagery, forest canopy gaps, understorey, vertical species diversity, microhabitat-bearing trees, contrast split segmentation, drone

1. Introduction

Forest canopy gaps are regarded as hotspots that provide ideal conditions for rapid plant reproduction and growth, maintenance of floristic richness in the understorey and increase of diversity and structural complexity of forest habitat [1]. Gaps dynamics, associated to the fall of

individual or clumped canopy trees, are observed in boreal, subalpine, temperate and tropical forest types worldwide, especially in late stages of forest development [2–5]. The idea to trigger gap dynamics is at the root of gap-based close-to-nature silviculture in managed forests [6,7].

Small canopy openings might be attributed to tree crown architecture, namely intra-crown porosity and to the space among crowns. Even in fully stocked forest areas, for some tree species the so-called 'canopy shyness' phenomenon can be observed, characterized by a canopy cover with inter-crown cracks running through it. However, little is known about the relationships between this fine-scale pattern of canopy openings, the sunlight penetration into the canopy, and their impact on the forest understorey layer.

Remote sensing from unmanned aerial vehicles (UAV) allows the detection of small size canopy gaps spatial patterns [8]. Since the optimal spatial resolution of the sensor is suggested to be five times smaller than the monitored object [9], the new versatile imaging platforms (UAV) offer a high potential for exploring canopy features at very high spatial resolution. UAVs have many benefits in forest remote sensing, such as the flexibility to acquire one's own data with low material and operational costs, and the high intensity data collection [10].

However, the use of UAVs is hindered by a set of challenges such as coverage of small areas per single flight due to low flight altitude, limited battery capacity, and existing regulatory requirements to keep the UAV in visual line-of sight (VLOS) of the pilot. Nevertheless, lightweight fixed wings UAVs allow to cover a larger area with one flight (up to 150 ha) than multicopter drones. Furthermore, the use of multiple batteries on lightweight fixed wings UAV may lead to cover up to 1000 ha in one working day, under optimal weather conditions [11].

UAVs can be equipped with a variety of sensors [12]. In recent years, practitioners have gained interest in UAVs applications in forestry either by using solely optical cameras [12–15] or by combing them with Structure for Motion Photogrammetry (SfM) [11,16], which offered new possibilities to easily derive 3D data (e.g. image-based point cloud) [13,14,17] and 2D data (e.g. digital surface model and orthomosaic) from UAV imagery.

UAV 3D image-based point clouds, normalized by high resolution Digital Terrain Model (DTM), has been explored for the estimation of forest structural variables (e.g. tree density, growing stock or above ground biomass), as a cheaper alternative to airborne laser scanning [13,18,19]. Whereas, UAV orthomosaic applications cover the detection of canopy openness [20], tree species identification [21] and assessment of infestation and damages at tree level [22–25].

Most studies opted for wall-to-wall fine scale mapping of forest canopy attributes over small forest areas [13,26–32]. Instead, classification of UAV orthomosaics to extract covariates, like canopy gaps-related metrics, potentially correlated with compositional and structural biodiversity variables has been less explored. Indeed, the definition of canopy gap itself remains unclear and inconsistent in the literature [33,34]. In addition, although it is known that gap size and shape considerably influence gap microclimate [1,35], still unambiguous indication of thresholds for these gap metrics is lacking [35]. In their study, Bonnet et al. [36] defined canopy gaps as 'openings in the canopy with a minimum area of 50 m^2, a minimum width of 2 m and a maximum vegetation height of 3 m'. Getzin et al [37] adopting a different definition, achieved to map canopy gaps of the size of 1 m^2 from a true colors UAV product of 7 cm spatial resolution, in beech dominated deciduous and mixed deciduous-coniferous forests in Germany. Furthermore, Getzin et al. [8] extracted forest gaps and their spatial pattern from ten different plots of 1 ha. The authors recommend collecting aerial data in a cloudy condition, in order to reduce the effect of the shadow that could lead to the misinterpretation of dark pixels as gaps.

Likewise, gap age is important since canopy openings fill with time and the biodiversity is disparate between a newly opened gap and an old one [1]. In addition, according to Muscolo et al. [6], canopy gap age and size are the primary factors affecting the regeneration besides the suitable substrate. As to UAV imagery classification for gap mapping, techniques and packages developed for the airborne and satellite images hardly suit because of different data acquisition parameters [38,39]. Although some studies tried to overcome some of the challenges [8,20,37], they used methods rarely available at low cost or handy for forest managers.

Since lightweight fixed wings UAV, equipped with a digital commercial RGB camera are most common in forest remote sensing [12,13], testing their use for exploring correlations between canopy openness and the occurrence of key forest biodiversity features in the understorey and overstorey, seems as an interesting opportunity. This is attempted in this study carried out in a small test site covered by temperate deciduous forests in central Italy. An integrated survey combining RGB imagery acquisition by UAV, with field-based forest inventory was conducted at an experimental site in 2016, in the framework of the LIFE project "FREShLIFE - Demonstrating Remote Sensing integration in sustainable forest management". Gathered data were processed in the present study, in order to explore relationships between canopy gaps and certain variables describing the structure and diversity of forest stands and of the understorey. Specifically, we examined the following questions:

Q1 – Is it possible to identify handy image processing techniques to delineate openings in the canopy cover from UAV imagery?

Q2 – Are patch metrics of these canopy features correlated with structural and biodiversity-related variables of the forest understorey or of the forest stand? Does this correlation vary across stands characterized by different dominant canopy species?

2. Materials and Methods

2.1. Study site

The test site extends over 240 hectares on the slopes of Mount Venere (500-800 m a.s.l.), in Caprarola Municipality (Central Italy). The site is covered by three forest types (Figure 1): beech dominated forest (*Fagus sylvatica,* 149 ha), turkey oak forest (*Quercus cerris*, 76 ha) and mixed forest of the two species (14 ha). Vertical profile is, to a large extent, monolayered in the beech forest and bi-layered in the other two forest types.

The presence of very fertile volcanic soils and the particular microclimate, related to the presence of the lake, create favorable conditions for the growth of beech, even at a low elevation. In fact, the conformation of the basin, the frequent formation of mists, the high relative air humidity and the protection from extreme winds ensure a suitable habitat for this species. As result, the beech forest of Monte Venere has a relevant ecological importance as it grows at much lower altitudes (around 500 m above sea level) than those usually occupied by beech in the Central Apennines (optimum between 1,000 and 1,700 m asl).

Beech forest of Monte Venere belongs to the *Aquifolio-Fagetum* association, that seems to reach the extreme northern boundary of its ecological range in the Province of Viterbo [40]. Beech is usually accompanied by other deciduous trees like *Quercus cerris* L. (turkey oak) - in the upper layer and only at lower altitudes, *Carpinus betulus* L. (hornbeam), *Castanea sativa* Mill. (Chestnut), *Acer opalus* L. (maple), *Corylus avellana* L. (hazel), *Ilex aquifolium* L. (holly) - in the dominated in layer -.

Turkey oak becomes the dominant species in the reliefs facing south. Turkey oak forests also contain accompanying species such as ash (*Fraxinus ornus* L.) and hornbeam (*Ostrya carpinifolia* L.). Turkey oak forests present a well-developed shrub layer including *Rosa canina* L., *Cornus sanguinea* L., *Crataegus monogyna* Jacq., *Crataegus oxychanta* L., *Ruscus aculeatus* L.

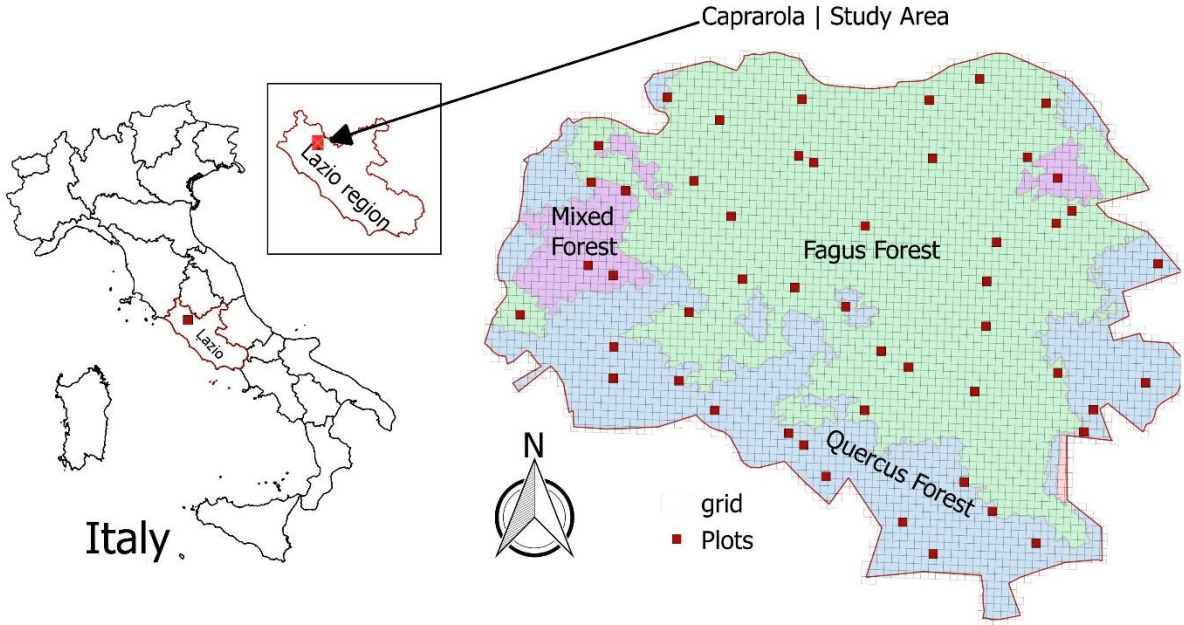

Figure 1. Location map of the study area with the three main forest types and the 50 samples (plots) location

The test site contains fifty squared forest inventory plots of 23 meters' side (area of the plot 529 m^2) distributed according to a one-per-stratum systematic sampling design. This sampling scheme envisages to partition the study area into a grid of squared 529 m^2 plots spatially aggregated into N (in our case N=50) equal size strata. One sample-site location is independently and uniformly selected in each stratum, resulting in the spatial distribution displayed in *Figure 1*. There were 28, 13, and 9 plots in beech, turkey oak, and mixed forests, respectively.

2.2. Field data processing

The spatial position of the center of inventory plots was recorded with GNSS receivers with a sub-meter accuracy. At each plot, all plants (trees and shrubs) with a diameter at breast height (DBH) greater than 2.5 cm were inventoried during the 2016 growing season. Key measurements included species identification, diameter at breast height (DBH), tree height, and the presence of microhabitat-bearing living trees according to the reference catalogue provided by Winter and Möller [41]. These elements characteristic of natural forests, especially of the old-growth phases, are often absent or rare in managed forests and are therefore considered key indicators of biodiversity.

Tree and shrub data were processed in the present study to distinguish plants of the understorey from canopy trees (living trees). The understorey layer was identified as the one including plants with height up to the 50% of the maximum tree height observed in the plot [42]. In each plot, we calculated for the understorey:

i) density and development, by means of the parameters such as number of plants (N_PLANTS), mean DBH (MEAN_DBH), mean plant height (MEAN_HTOT), total basal area (G_TOT) and total understorey volume (V_TOT);

ii) species diversity, by means of number of species (N_SPECIES), Shannon index (I_SHANNON, H') [43], Pielou index (I_PIELOU) [44],.

Data collected on living trees were processed to derive structural data (mean dbh, MEAN_DBH; mean total height, MEAN_HTOT) and biodiversity data such as number of habitat trees (HAB), percentage of habitat trees (%HAB) out of total plants in the plot, vertical species profile by the index of Pretzsch (I_PRETZSCH), the index of Shannon (I_SHANNON), the index of Margalef (I_MARGALEF) [45]. Table 1 displays the summary of biodiversity indices computed for each plot.

Peer-reviewed version available at Remote Sens. 2018, 10, 1397; doi:10.3390/rs10091397

Table 1. Summary of diversity indices

Indices	Formulae	Range of variation	Description
Shannon index (H')	$-\sum p_i \ln(p_i)$	[0,ln(S)]	It expresses the frequency of the i-th species in a community, takes values generally between 0 and 3.5; higher values correspond to higher species diversity. Its maximum value (MAX_SHANNON) is given by the natural logarithm of the number of species found in the test area and occurs when all species are equally present.
Pielou index (E)	$H'/\ln(S)$	[0,1]	The index measures the relative abundance of species groups. The index can take values between 1 (all species are equally abundant) and 0 (there is only one species).
Pretzsch index (A_p)	$-\sum_{i=1}^{S}\sum_{j=1}^{Z} p_{ji} \ln(p_{ij})$	[0,ln(SxZ)]	The index summarizes and quantifies species diversity and the vertical distribution of species in a forest. The index is lowest in one-story pure forests, whereas it rises for pure forests with two or more stories. Peak values are reached in mixed woodlands with heterogeneous structures.
Margalef index (D)	$(S-1)\ln(N)$	[0,∞)	It quantifies the presence of a number of species in a community. It also depends on the number of plants found in the sampling area. The index grows with increasing species diversity.

S=number of species; *N*= total number of plants; *pij*= the frequency of specie *i* in the layer *j*; *pi*= frequency of the specie *i*. *z*= number of layers

2.3. UAV data

Aerial images covering the test site area were collected near peak greenness during two consecutive days of the last week of May 2016 by the fixed-wing eBee drone (SenseFly, Cheseaux-Losanne, Switzerland). The eBee was equipped with a commercial SONY WX 18.MP RGB camera, with sensibility in blue (450 nm), green (520 nm) and red (660 nm). The eBee, a hand-launched fixed wing drone with an electric motor-driven pusher propeller, has a 96 cm wingspan and a weight of about 700 g including camera, inertial measuring unit, GPS and battery payloads. The maximum area covered in a single flight is about 140 ha at 120 m altitude or 9 km² at 2000 m altitude, with a maximum flight time of 45 min.

Before UAV acquisition, 15 ground control points (GCPs) were placed in open areas on the ground using 50x50 cm targets with a black and white chalkboard pattern, in order to ensure high visibility on the images. The coordinate of GCPs where recorded with a Trimble Geo 7X receiver, with a 2-second logging rate for approximately 15 minutes each. The recorded coordinates were post-processed with data from the nearest ground station, located at 30 km from the study area, using Pathfinder software. The post-processed GCP coordinates resulted in an average standard deviation from northing, easting and height of 0.9 m, 0.7 m and 1.9 m, respectively.

Flight altitude was set on 145 m above ground level, and the flight lines were set to obtain a longitudinal overlap of 85% and lateral of 75%. The total flight time was 2 hours and 43 minutes divided into eight flights, landing from two different areas. Flight line spacing was 42 m and the distance between two adjacent photos was 34.6 m. The focal length of the camera was set to 4 mm

and the ISO sensibility was ISO-100 with a shutter speed of 1/2000 sec. A total of 433 images were acquired with a field of view of 200 m x150 m.

The visual inspection of the acquired images revealed no problems related to light and atmospheric conditions, saturation. Orthomosaic data were derived from the UAV images using the SfM photogrammetry software Agisoft PhotoScan Pro [46]. This software allows to fully automate the photogrammetric workflow to process aerial images and produce 3D (e.g. image-based point cloud) and 2D (e.g. Digital Surface Model and Ortomosaic) models, thanks to the multi-view stereo-matching and SfM algorithm implemented.

This software has been already used for forest analysis [11,13,47–50] and the UAV images were processed as follows: (a) image alignment; (b) mesh building; (c) guided marker positioning and optimization of camera alignment (georeferencing of created scene), (d) dense cloud building and (e) raster grid DSM generation with a resolution of 0.2m x 0.2m, (d) building orthomosaic. The steps involved in Photoscan's pipeline process and their relative parameterization are presented in *Table 2*. From the SfM photogrammetric workflow we obtained a raster grid orthomosaic with a spatial resolution of 10 cm.

Table 2 - Processing steps with corresponding parameters in Photoscan's pipeline process for the generation of orthomosaic from UAV imagery; a: parameters chosen in accordance with Puliti et al.[13]*; b: parameters chosen using the trial and error approach.*

Task	Parameters
Align photos	Accuracy: high [a] Pair selection: reference [a] Key point limit: 40000 [a] Tie point limit: 1000 [a]
Build mesh	Surface type: height field [b] Source data: sparse point cloud [a] Face count: low (13544) [a] Interpolation: enabled [a]
Guided marker positioning	
Optimize camera alignment	Marker accuracy (m): 0.005 [a] Projection accuracy (pix): 0.1 [a] Tie point accuracy (pix): 4 [a] Fit all except for k4 b Number of GCPs: 15 [b]
Build dense cloud	Quality: Medium [a] Depth filtering: mild [a]
Build Digital Elevation Model (DEM)	Source: Dense Point cloud [b] Interpolation: Enabled [b] Resolution pixel (m): 0.20x0.20 b
Build Orthomosaic	Surface: DEM [b] Blending mode: Mosaic [b] Pixel size (m): 0.10x0.10 [b]

2.3. *Methodology for answering research questions:*

The key methodological steps for addressing initial research questions were to:

(Q1): 1. segment the orthomosaic to delineate canopy openings and process gap patch metrics;

(Q2): 2. perform exploratory statistical analysis on structural and biodiversity variables, processed from field data, for testing group differences among beech- turkey oak dominated forest and mixed forests; this step allowed to determine whether the field sample should be stratified into forest types for subsequent correlation analysis between a field variable and gap metrics.

3. model field variables correlated with gap metrics by linear regression, at the forest type level for purpose of producing local spatial estimates of structural and biodiversity variables.

Peer-reviewed version available at Remote Sens. 2018, 10, 1397; doi:10.3390/rs10091397

The overall flow chart of the methodology is presented on Figure 2.

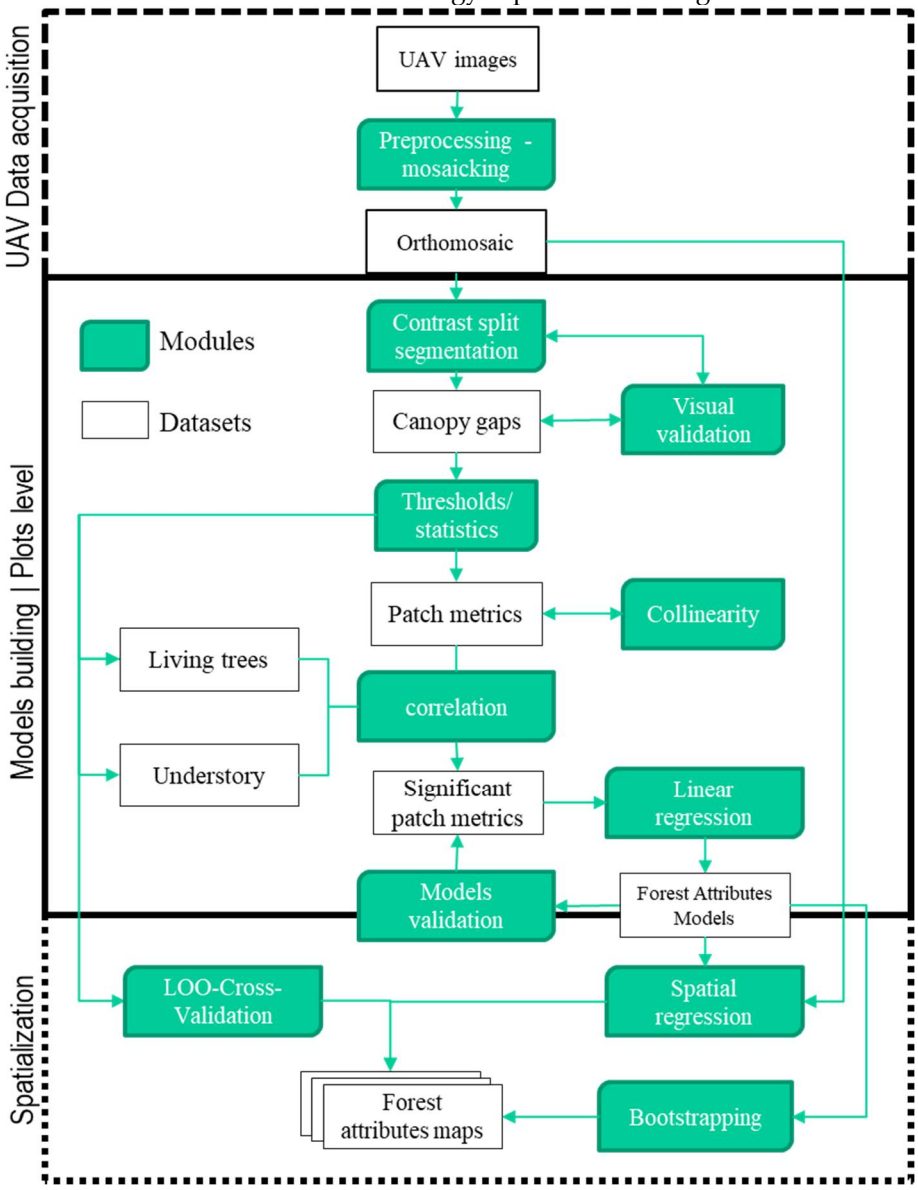

Figure 2. Flow chart of the methodology

2.3.1. Image processing and variable selection

We tested different settings of the Contrast Split segmentation algorithm to map forest canopy openings from the red band of the RGB orthomosaic. The red band was the only one significantly contrasting openings in the canopy cover and the crowns. The Contrast split algorithm is considered effective in separating dark objects from bright ones [51]. The idea of testing different settings is to extract as accurately as possible forest canopy openings, which are expected to appear darker, compared to surrounding canopy pixels. This process was accomplished using eCognition Developer (http://www.ecognition.com) software. We validated the gap delineation from contrast split segmentation, by visual interpretation of the orthomosaic, to look for omission or commision errors. The visual validation techniques have been often used in forest canopy gaps mapping [33]. We later tested different thresholds to discriminate small openings which might not affect ecological phenomena under investigation and therefore constitute a noise masking relevant data. We only considered mapped features falling within the plot boundary and gaps within the plot boundary for at least 50% of their area. For each feature, we calculated shape and size indices, and other gap patch metrics commonly used in landscape-scale analyses. In total 19 patch metrics (see Supplements; more details in [52]) were processed for each single gap in each plot. This suite of metrics reflects different

Peer-reviewed version available at Remote Sens. 2018, 10, 1397; doi:10.3390/rs10091397

nuances of two- dimensional gap properties that may be potentially important for linking image-detected higher-level structures to dependent lower- level processes of the biota [37].

The size or extent gap patch metrics are the area (*A*), the length, the border length (or the perimeter), the ratio length/width, the width. The shape ones are border index (*B.Index*), asymmetry (*Asym*), roundness (*Round*), compactness (*Comp*), shape index, density, rectangular fit (*Rect.fit*), radius of the largest enclosed ellipse (*RLE*), radius of the smallest enclosed ellipse (*RSE*), elliptic fit and other composite indices such as the shape complexity index (*GSCI*). The gap shape complexity index is an important measure of forest gaps [53]. It is the ratio of a gap's perimeter to the perimeter of a circular gap of the same area. A value of 1 describes a perfect circle while increasing values indicate increasing shape complexity. For example, values of 1.20 and 2.70 have 20% and 170% complexity, respectively. The last three gap metrics are the patch fractal dimension (*PFD*) [54], the fractal dimension (*FD*) [55] and the fractal dimension index (*FDI*) [56]. A description of each metric and its range of variation is given in *Table 6* (Appendix).

For each patch metric, we calculated the median (mdn), the mean (avg), the standard-deviation (SD), the sum (SUM), and the coefficient of variation (cv) per plot. We tested gap metrics with two different gap size thresholds namely greater than 1 m^2 and greater than 2 m^2. This leads to two times 95 variables for each plot. These two thresholds were set because some ecological phenomena, such as understorey structure dependencies, are only quantifiable if small gaps are taken into account, yet very small gaps may not affect at all the lower dependency phenomenon, constituting, therefore, a noise [57].

2.3.2. Statistical analysis

Firstly, we performed exploratory analysis on field data by computing the ANOVA (Analysis of Variance) when the distribution is normal and the KRUSKAL-WALLIS analysis otherwise, with the categorical variable being the forest type characterizing each single plot.

We used all gap variables for Pearson's product-moment correlation analysis and Spearman's rank correlation with the field data, using post-stratification of sampling units by forest types where appropriate. Usually, the two correlations give approximately the same results (see [58]). To avoid that the observed correlation, although significant according to the p-value lower than 5%, could have occurred by chance, its significance was further thoroughly tested using the 9999 permutation method proposed by Legendre and Legendre [59]. This method has been successfully used by some researchers investigating the relationship between forest canopy gap metrics and biodiversity [37].

For gap variables correlated with field data, we tested the correlation among significant potential predictors. This third step allowed to decrease the redundant information brought by correlated potential predictors and eliminate the collinearity or singularity. To determine the most significant variables to be used as possible predictors we used a forward stepwise analysis since this approach select only the minimum significant number of predictors. There exist three methods for model selection known as best, forward and backward subset selection. In general, the three methods lead to similar though not identic results [60]. Owing to the huge number of predictors (190 in this study), the use of best selection will require for each field parameter to compare up 2 power of 190 models, which deter from using the best set selection.

When the forward stepwise yielded only one predictor variable as sufficient to model the field parameter (which was often the case), we compared the correlation coefficients of Spearman and Pearson. If these two coefficients were significant and close to each other, then the patch metric is selected as a predictor if it passes the 9999 permutations test of Legendre. Otherwise, the second variable denoting both Spearman and Pearson coefficients significantly high is selected and the we repeat the 9999 permutations. This approach has the advantage of, on the one hand, excluding variables depicting high Pearson's correlation due to extreme values, and on the other hand, not solely relying on the Spearman's correlation which is a measure of monotony [61] and not of linearity. The 9999 permutation assures that the p-value observed does not occur by chance.

Finally, we performed the linear regression using the selected significant variables. Following the lines of Møller and Jennions [62] and Getzin et al. [37], who considered a coefficient of determination $R^2 > 0.25$ as meaningful since the predictor value leads to a great change if it explains over 25% of variance, we set as threshold $R^2 > 0.5$. We then validated the regression by checking the regression quality assumptions such as the normality of residuals, the homoscedasticity of residuals, the mean of the residuals is zero. Statistical analyses were performed with R Foundation 3.2.3 (https://www.r-project.org/foundation/). For forest parameters which can be predicted with R^2 greater than 50%, we generalized the model to the whole forest type extent using the grid of squared 529 m^2 plots. We performed the validation with cross-validation (Leave-One-Out Cross-Validation) producing hence the root mean square error (RMSE).

For inference, it is important to provide the variance, the confidence interval, and the bias of R^2. Bootstrapping is the method commonly used for that purpose [63–65] especially in the case of linear regression [66]. Bootstrap is a resampling method developed by Efron and Tibshirani [67]. We computed those statistics for variables with R^2 greater 0.50 using formulas given by Mura et al. [63]. Although it is suggested that the bootstrap sample size should be big enough (greater than 200), there is no consensus yet on what should be the actual size. Following the line of Mura et al. [63], we set the bootstrap sample size to 500. The mapping of biodiversity attributes was achieved with ArcGIS 10.2.

3. Results

3.1. Canopy gaps mapping

Q1 – Is it possible to identify handy image processing techniques to delineate openings in the canopy cover from UAV imagery?

The contrast split algorithm based on the red band managed to accurately differentiate dark objects (shaded canopy gaps) from bright ones which, in most cases, corresponded to forest canopy. The mapping faithfully delineated shaded canopy gaps but poorly performed in illuminated gaps when the bare soil was apparent (*Figure 3*). Detected gaps from plots ranged from 1 pixel (or 100 cm^2) to 122 m^2. This range encompassed small openings or inter-crown cracks in the canopy cover and larger gaps generated by the fall of one or more canopy trees. The gap size distribution is roughly the same in the three forest types. When considering gaps greater than 1 m^2, over 75% of gaps in the three forest types were less than 5 m^2. When considering gaps greater than 2 m^2, over 75% of gaps in the three forest types were less than 7 m^2 (*Figure 3*).

The collinearity analysis of gap patch metrics showed that patch metrics were strongly correlated to each other. A sample result of collinearity analysis of predictor variables is reported in Figure 4. The lowest correlations were obtained with the coefficient of variation, whereas the highest ones were associated to the plot-level sum of patch metrics. These findings indicate that gap patch metrics are not suitable for a multiple linear regression.

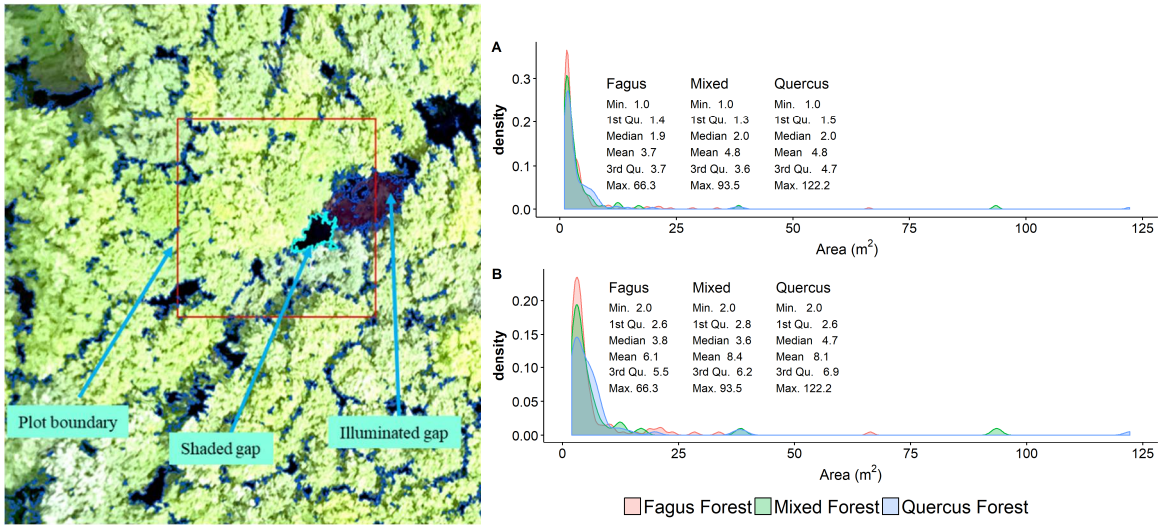

Figure 3. Snapshot of gap delineation using the Contrast Split algorithm (left). The size distribution of gaps limited to plots level (right). A: The minimal threshold of 1 m²; B: The minimal threshold of 2m².

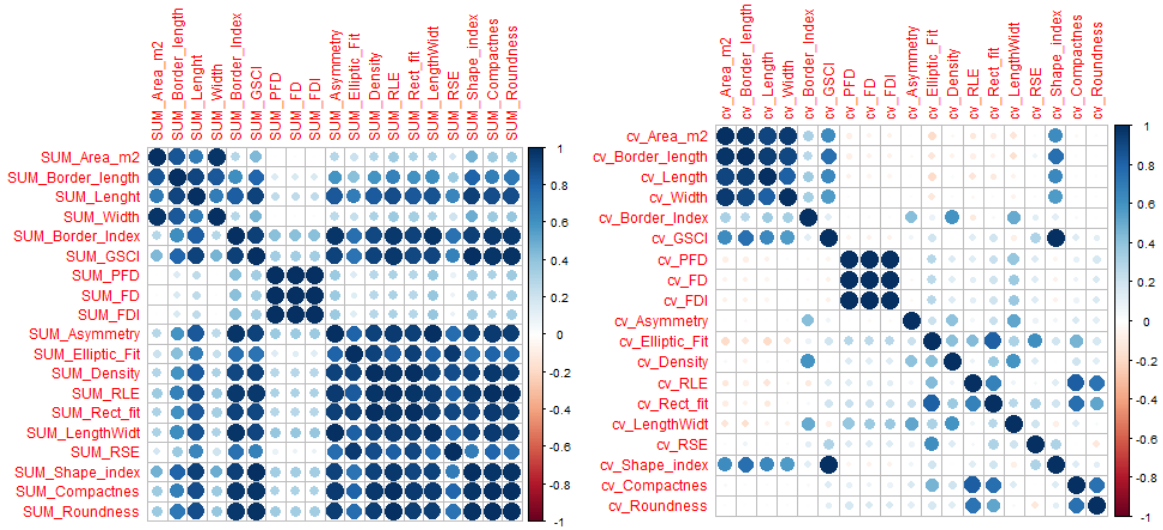

Figure 4. Example of the correlation matrix of the most correlated predictor variables and the least correlated ones. a) Correlation of Pearson from patch metrics variables associated with the sum and b) correlation of Pearson from the patch metrics associated with coefficient of variation.

3.2. Correlation between gap metrics and understorey variables

Q2 – Are patch metrics of these canopy features correlated with structural and biodiversity-related variables of the forest understorey or of canopy trees? Does this correlation vary across stands characterized by different dominant canopy species?

The understorey layer exhibits density, development and diversity features that seem to vary with forest types cover (Figure 5). Namely, variables related to the density, development and diversity of the understorey denoted significant differences amongst the forest types, except for Pielou index, MEAN_HTOT and MEAN_DBH (*Table 3*).

All the eight field parameters presented significant correlation ($p < 0.05$) with gap patch metrics in at least one of the three forest types (Figure 6). Tables 7-9 of Appendix B present the threshold, Pearson and Spearman correlations of gap patch metrics and understorey. The results of the regression indicated that regression coefficient had the lowest standard error in Mixed and Fagus forests compared to Quercus forest; MEAN_DBH in mixed forest had a very low variability as shown by the coefficient of the regression predicting MEAN_DBH in Mixed forest is merely equal to zero.

As shown in Figure 7, the highest coefficient of determination was in Mixed forest (MEAN_HTOT, $R^2 = 0.87$, $p < 0.000$) and the lowest was in Fagus forest (N_SPECIES, $R^2 = 0.15$, $p <$

Preprints (www.preprints.org) | NOT PEER-REVIEWED | Posted: 12 July 2018 doi:10.20944/preprints201807.0209.v1

Peer-reviewed version available at Remote Sens. 2018, 10, 1397; doi:10.3390/rs10091397

0.05). Best results were in Quercus and Mixed forest while the worst ones were in Fagus forest. I_SHANNON in Quercus forest, MEAN_DBH in Quercus forest, MEAN_HTOT and N_PLANTS in Mixed forest were predicted with R^2>0.50 (Figure 7). Patch metrics correlated with the field parameters were all but one (cv_Length in Fagus forest) related to gap shape.

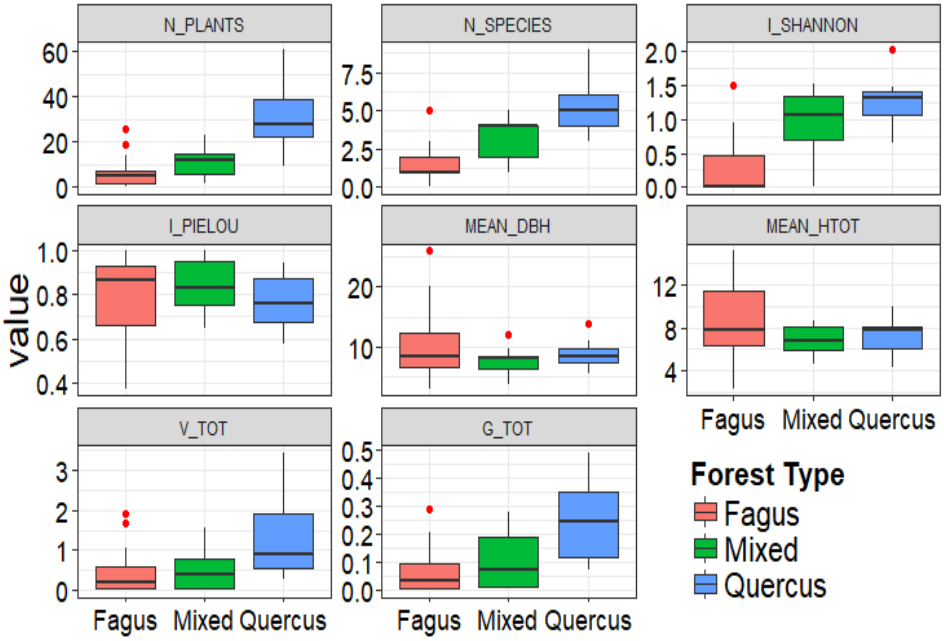

Figure 5. Variability of the understorey parameters amongst the three forest types.

Table 3. Summary of exploratory statistics on understorey data.

Normal distributed variables		
Variables	*ANOVA*	*TUKEY*
I_PIELOU	no significant difference	
MEAN_HTOT	no significant difference	
Variables non normal		
Variables	*KRUSKAL-WALLIS*	*MANN-WHITNEY*
N_PLANTS	***	(1 vs 2)***; (2 vs 3)**
N_SPECIES	***	(1 vs 2)***; (1 vs 3)**
I_SHANNON	***	(1 vs 2)***; (1 vs 3)**
MEAN_DBH	no significant difference	
G_TOT	***	(1 vs 2)***
V_TOT	**	(1 vs 2)**

*p<0,05; ** p<0,01; *** p<0,001; 1 = beech forest; 2 = oak forest; 3 = mixed forest

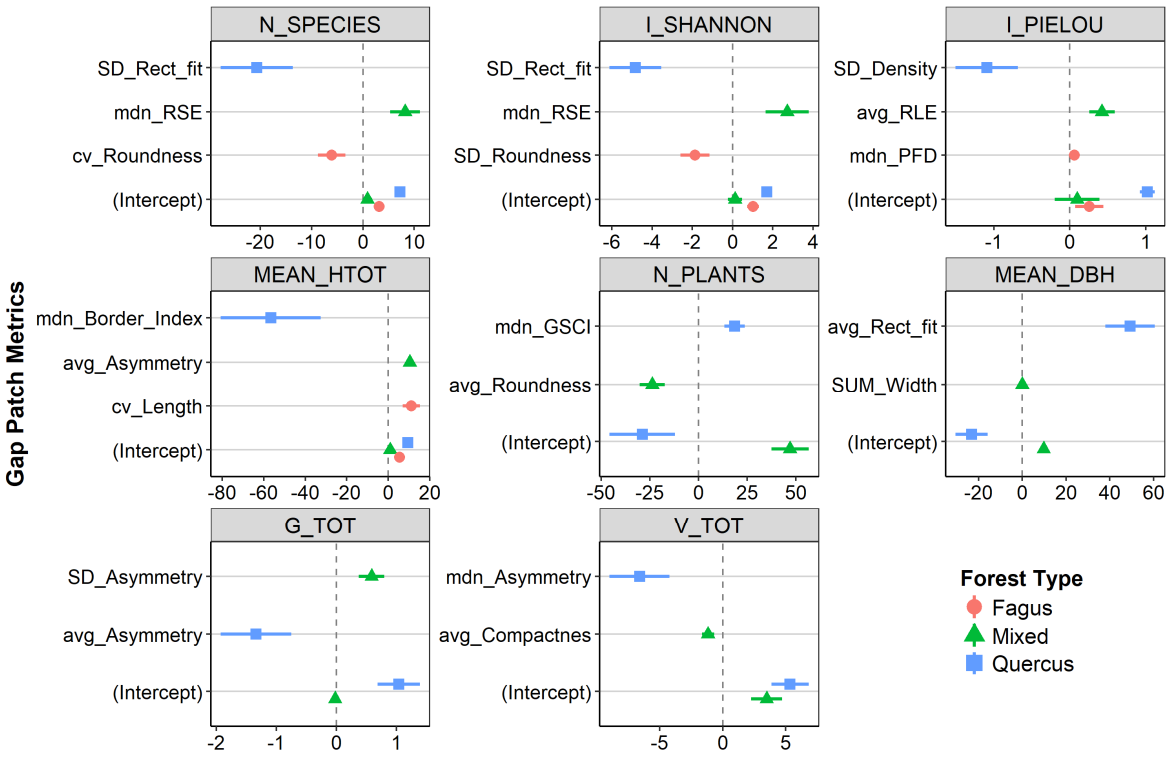

Figure 6. Coefficients of simple linear regression with the associated standard error of gap metrics predictors for the understorey parameters in the three forest types. For instance, N_SPECIES is explained in Quercus forest by an intercept and SD_Rect_fit

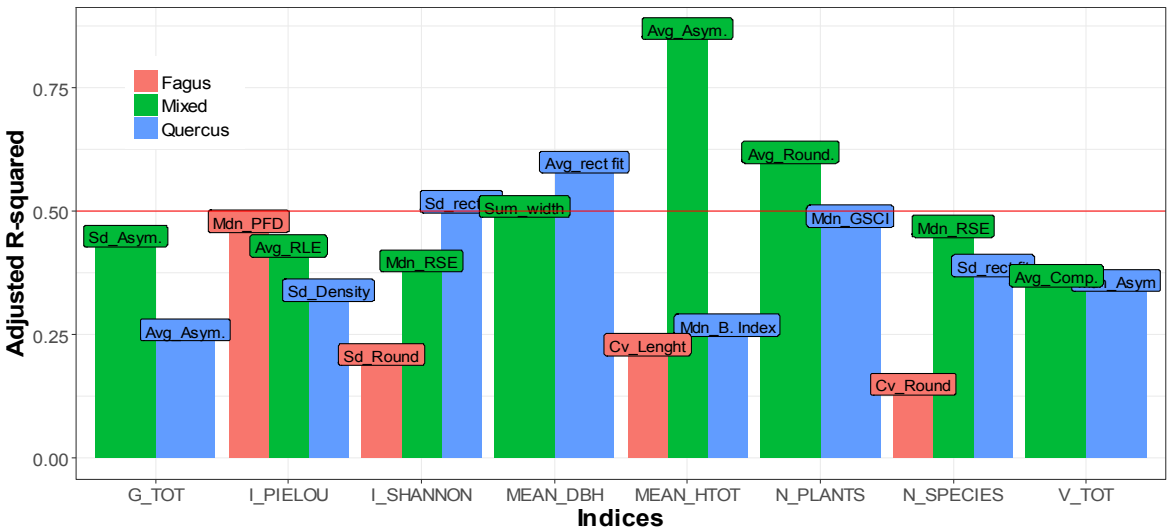

Figure 7. Summary bar chart of adjusted R^2 from linear regression with understorey data in the three forest types. On top of each bar is the patch metric which is the most correlated with the understorey parameter in the corresponding forest type.

The spatialization of the understorey models to the extent of their respective forest types underscored some key features (*Figure 8*). In Quercus forest, I_SHANNON ranged from just above 0 to 1.8 with RMSE of 0.21. These values are in the range of variation of data collected on plots. The range of variation of MEAN_DBH in Quercus forest was from 2 to 17 cm with an RMSE=1.3 cm.

In Mixed forest, MEAN_HTOT went up to 11 m, with the majority of grids falling between 5 and 9 m and the RMSE was 0.43. The number of plants per grid ranged from less than five to 33 with

an RMSE of 3.84 (*Figure 8*). We did not perform the spatialization of MEAN_DBH in Mixed forest even though the R^2 was greater than 0.5 because the linear model slope was close to zero. The empty cells in the figure corresponds to cells were the prediction gives unreasonable values.

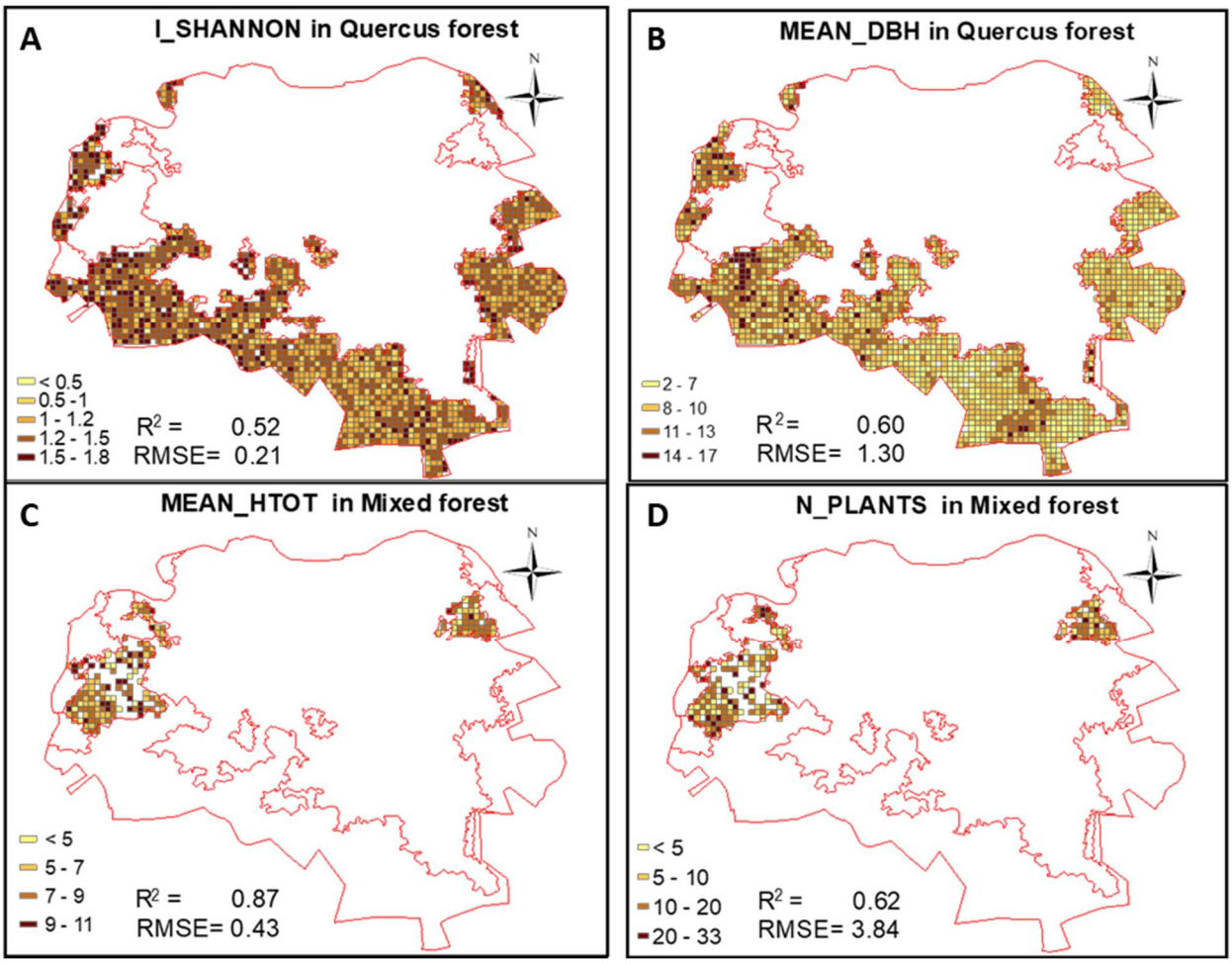

Figure 8. Spatialization of understorey parameters with R^2 greater than 50% in Mixed and Quercus forests. With predictor being: A- standard deviation rectangular fit; B- average rectangular fit; C- average asymmetry; D- average roundness

3.3. Correlations between gap metrics and living trees variables

All living tree diversity and structural variables denoted significant differences among the three forest types, except total basal area (G_TOT) and total volume (V_TOT) (*Table 4*). The range of variability of all the parameters is displayed in supplements (*Figure 9*).

As with the understorey, some gap patch metrics appear to be significantly correlated with these field parameters ($p < 0.05$) as shown in *Figure 10*. Tables 10-12 in Appendix C summarize the threshold, Spearman and Pearson Correlations associated with gap patch metrics and living trees parameters. In Quercus forest eight field parameters yielded good results, compared to Mixed forest which had four. For Fagus forest habitat trees and percentage of habitat trees only denoted significant correlations. Coefficients of the linear regression had the lowest standard errors in Quercus forest.

Preprints (www.preprints.org) | NOT PEER-REVIEWED | Posted: 12 July 2018 doi:10.20944/preprints201807.0209.v1

Peer-reviewed version available at Remote Sens. 2018, 10, 1397; doi:10.3390/rs10091397

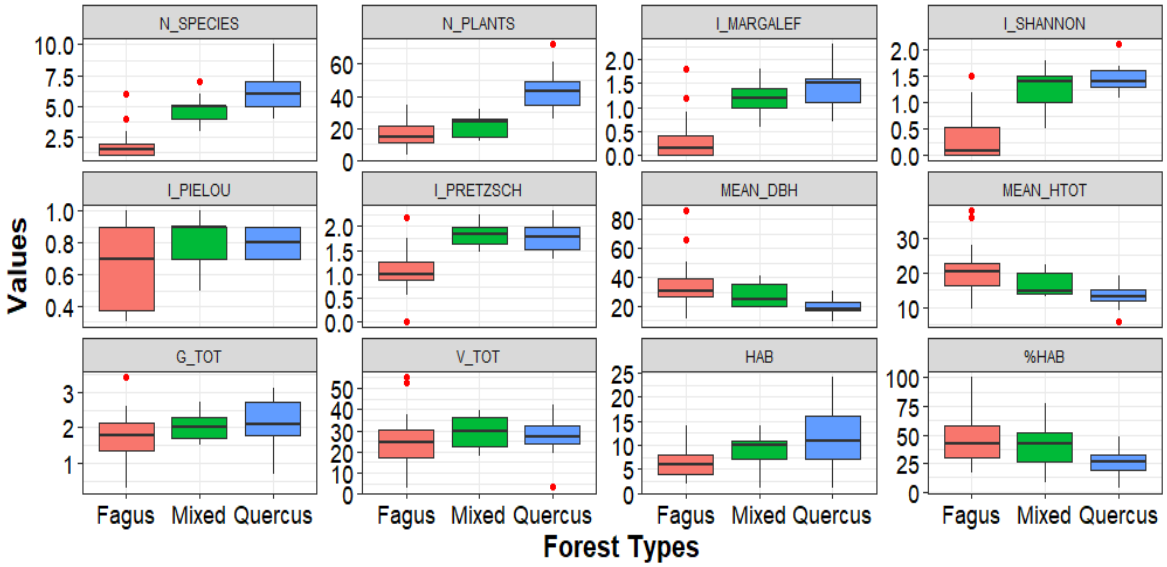

Figure 9. Boxplot of the living trees data per forest type

The highest coefficient of determination was in mixed forest (HAB, $R^2 = 0.79$, $p < 0.000$) and the lowest was in Fagus forest (%HAB, $R^2 = 0.11$, $p < 0.05$). Best results were in Quercus forest (I_PRETZSCH, HAB, %HAB) and Mixed forest (HAB, %HAB, MEAN_DBH, MEAN_HTOT). HAB, %HAB, MEAN_HTOT in Mixed forest, and HAB and I_PRETZSCH in Quercus forest had R^2 exceeding 0.50 (*Figure 11*).

Among the patch metrics correlated with living trees' parameters, except the length (cv_Length in Mixed forest), which is gap size related patch metric, all others were gap shape related patch metrics.

Table 4. Summary of exploratory statistics on living trees.

Variables with normal distribution		
Variables	*ANOVA*	*TUKEY*
N_PLANTS	***	(1 vs 2)***; (2 vs 3)***
I_PRETZSCH	***	(1 vs 2)***; (1 vs 3)***
G_TOT	no significant difference	
V_TOT	no significant difference	
HAB	*	(1 vs 2)**
%_HAB	**	(1 vs 2)*
Non normal distributed variables		
Variables	*KRUSKAL-WALLIS*	*MANN-WHITNEY*
N_SPECIES	***	(1 vs 2)***; (1 vs 3)***
I_MARGALEF	***	(1 vs 2)***; (1 vs 3)***
I_SHANNON	***	(1 vs 2)***; (1 vs 3)***
MEAN_DBH	***	(1 vs 2)***; (2 vs 3)***
MEAN_HTOT	**	(1 vs 2)**

*p<0,05; ** p<0,01; *** p<0,001; 1 = beech forest; 2 = oak forest; 3 = mixed forest

Preprints (www.preprints.org) | NOT PEER-REVIEWED | Posted: 12 July 2018 doi:10.20944/preprints201807.0209.v1

Peer-reviewed version available at Remote Sens. 2018, 10, 1397; doi:10.3390/rs10091397

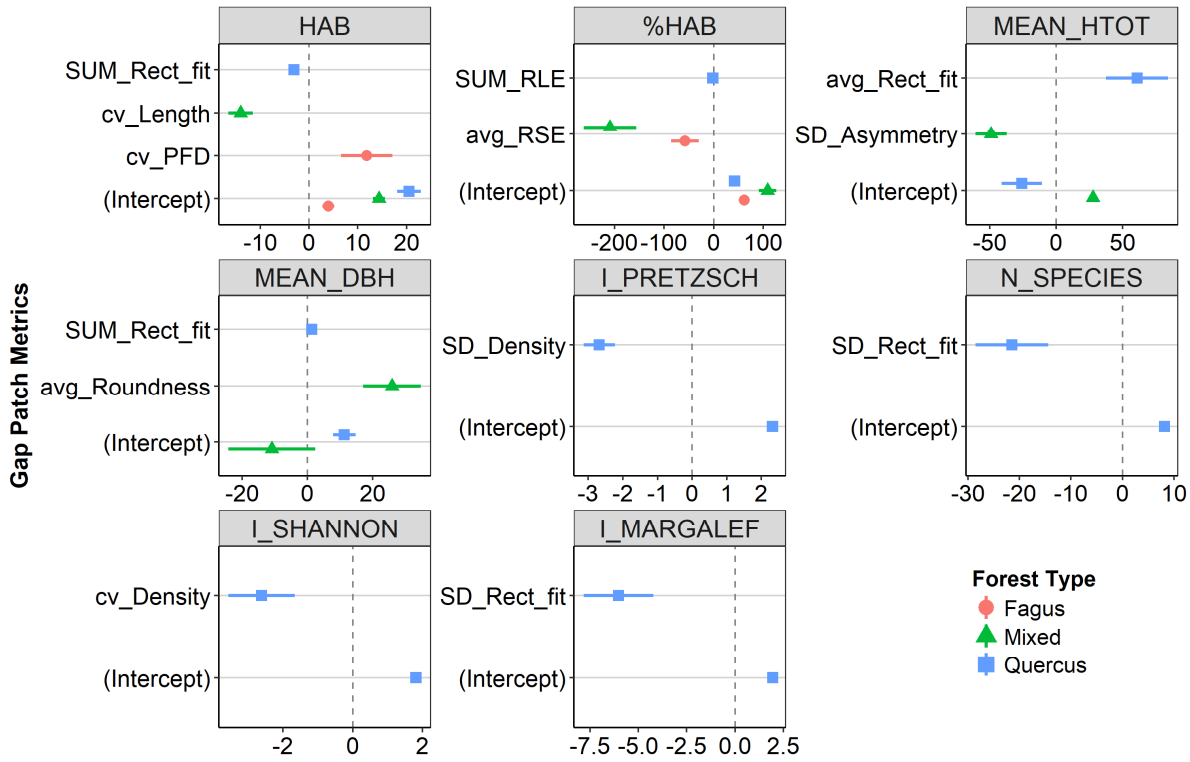

Figure 10. Coefficients of simple linear regression with the standard error associated for living trees parameters in the three forest types. For instance, the number of habitat trees (HAB) is explained in Fagus forest by an intercept and cv_PFD.

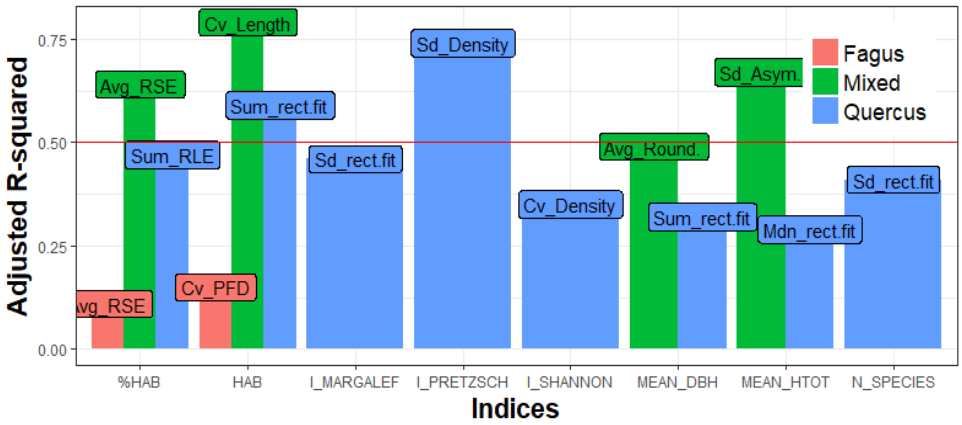

Figure 11. Summary bar chart of adjusted R^2 from linear regression with living trees data in the three forest types. On top of each bar is the patch metric which is the most correlated with the living trees parameter in the corresponding forest type.

The spatialization of regression models for living trees parameters is presented in *Figure 12*. In Quercus forest, I_PRETZSCH varied from 1 to 2.4 with RMSE of 0.40. The majority of cell grid had the index higher than 1.7 indicating a complex vertical structure. In the same forest type, the number of habitat trees reached 20 with RMSE of 3.89.

In Mixed forest, however, most of cell grids had the number of habitat trees higher than 9. In this forest, the prediction error is relatively smaller with an RMSE of 1.6. The percentage of habitat trees per grid is more variable with values ranging from 0 to 100%. The MEAN_HTOT varied from 6 to 28 m with an RMSE of 1.86.

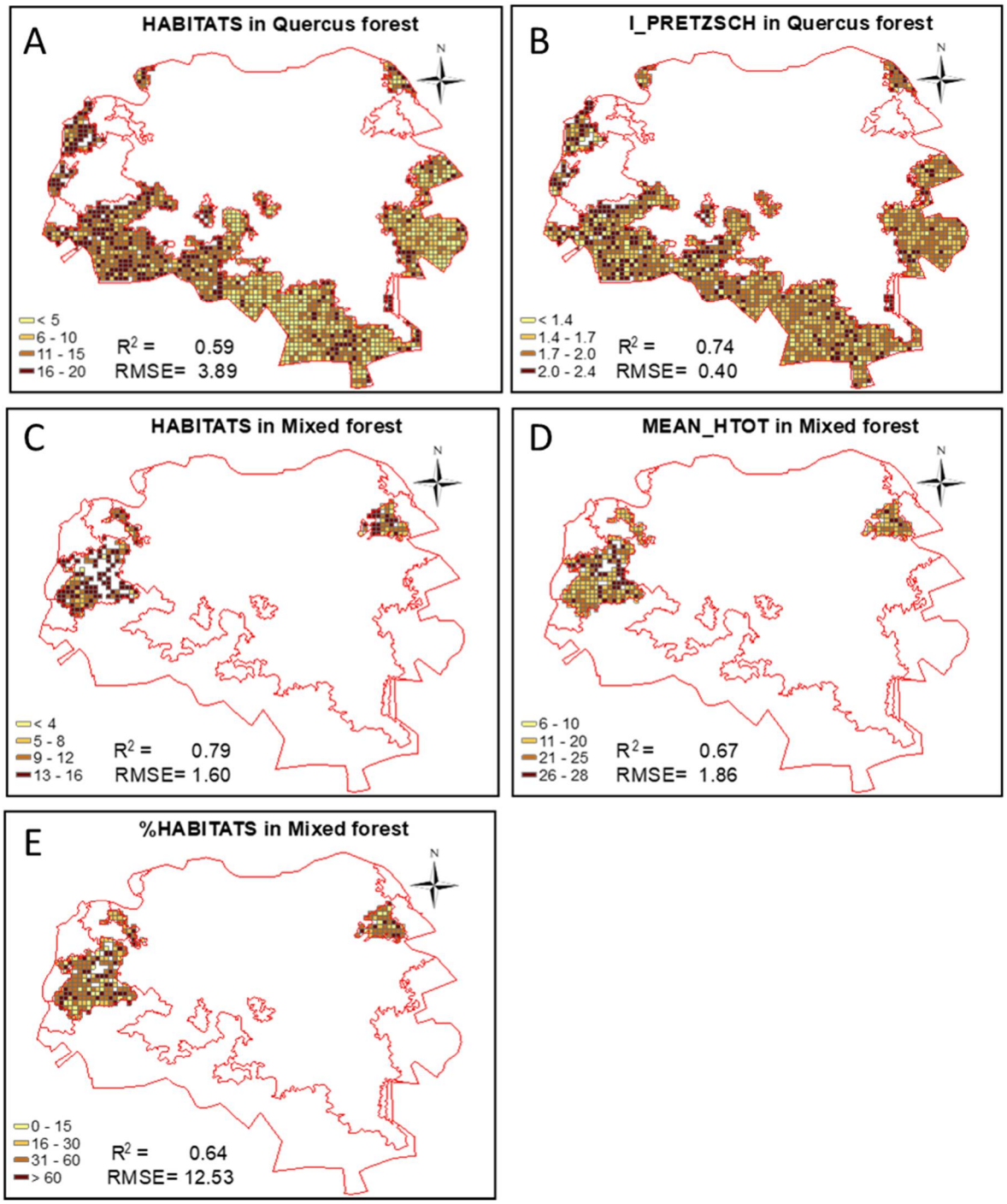

Figure 12. Spatialization of living trees parameters with R² greater than 50% in Mixed and Quercus forests. A: Habitat trees in Quercus forest; B: Pretzsch index in Quercus forest; C: Habitat trees in Mixed forest; D: Mean total height in Mixed forest; E: Percentage of habitat trees in Mixed forest.

3.4. Results quality assessment

The bootstrap R² was relatively close to the experimental R² (computed from the actual data) for both the understorey and the living trees. The standard error and the bias are very low. The highest negative bias was related to I_SHANNON with a bias of -0.05. This means that the actual R² of I_SHANNON is lower than the one observed. Similarly, the highest positive bias was recorded with HAB in mixed forest (living trees with a value of 0.03). This suggests that the actual R² associated to habitat trees in mixed is higher than 0.79 (*Table 5*).

Table 5. Resuts of bootstrapping for parameters with R^2 greater than 0.50

	Forest types	Parameters	Bootstrap R^2	Standard error (95%)	R^2	Bias
Understorey	Mixed	MEAN_HTOT	0.877	0.006	0.872	-0.005
		N_PLANTS	0.623	0.016	0.616	-0.007
		MEAN_DBH	0.507	0.022	0.515	0.008
	Quercu	MEAN_DBH	0.577	0.017	0.600	0.024
		I_SHANNON	0.576	0.010	0.523	-0.053
Living trees	Quercus	PRETZSCH	0.755	0.008	0.738	-0.016
		HAB	0.554	0.018	0.586	0.032
	Mixed	MEAN_HTOT	0.682	0.012	0.674	-0.008
		HAB	0.757	0.014	0.790	0.032
		%HAB	0.627	0.019	0.644	0.017

4. Discussion

4.1 Mapping forest canopy gaps

Gap mapping from UAV RGB 10 cm orthomosaic seems to produce very promising results. In this study, we accomplished mapping openings in canopy as small as 100 cm^2, corresponding either to intra-crown openings or to inter-crown cracks in the canopy cover. This fine-scaled mapping of canopy openings is important because some ecological phenomena, such as understorey structure dependencies, are only quantifiable if small gaps are taken into account. Since there is not yet a rule for minimum gap size, different authors set, arbitrarily a minimum gap size of 1 m^2 [8,37,57,68–70], 5 m^2 [71], 10 m^2 [33,72] and 50 m^2 [36]. To circumvent this problem, we did not set any gap size limit but let the ecological phenomenon under investigation dictate the appropriate gap size limit. Hobi et al. [73] used the same approach by not setting any gap size limit. The gap mapping used in this paper does not take into account the vegetation height. Therefore, our mapping, although consistent with the definition given by Brokaw [74], focusses only on shaded gaps or dark objects. Zielewska-Büttner et al. [33] reported as well that in their attempt to map forest canopy gaps, the shadow occurrence and forest height affected the mapping accuracy.

Other authors who mapped forest gaps from remote sensing used either LiDAR-derived forest canopy height models [53,68,70,75–77], or RGB imagery photogrammetric derived canopy height model (CHM) [33,34,75,78]. Alternatively, fish eye [79], airborne lidar derived data [76,80] or terrestrial laser scanning [81] can be used. All those techniques, although effective, are not affordable for small forest land owners.

Furthermore, the forest canopy mapping was highly affected by the quality of the orthomosaic and images acquisition conditions. In this study, the orthomosaic co-registration presented some flaws in certain areas. Those areas denoted a low quality in gaps delineation and even in the visual interpretation of what constitutes a gap. The second limitation came from the difference in reflectance between the datasets acquired in the two consecutive days. Although the images were acquired at noon to reduce the bidirectional reflectance effect [22], the sun illumination between the two days was not the same, leading thus to two sets of images with slightly different brightness. The best practice would be to collect data covering the site in the same conditions and, if possible, in the same day.

Finally, the contrast split algorithm utilized failed to detect illuminated canopy gaps where the bare soil is visible, because the bare soil reflectance is as high as the one of the vegetation. Therefore, the algorithm missed big gaps with no vegetation but with apparent bare soil. As an alternative, multiresolution segmentation would allow to detect both types of canopy gaps, though it requires all image objects to be subsequently classified by the user (more time consuming than contrast split). The second alternative would be to use image based 3D point clouds. This dataset, possessing a third

dimension, is sufficient for detecting local minima in the digital crown model, e.g. by means of hotspot analysis [82].

4.2 Modeling understorey variables through canopy gaps covariates

The very high-resolution mapping of gaps in the canopy cover, provided a set of metrics that proved to be useful as covariates in regression estimation of the density (number of plants), the diversity (Shannon index) and the development (mean DBH, mean HTOT) of the understorey in Quercus and Mixed forest types. The same cannot be said for Fagus forest. A general explanation for this lies in the different light conditions under Quercus and Fagus canopy cover. The crown of Turkey oak, when grown in fully stocked high forest, is oval-shaped, high inserted and medium-textured. Due to this structure this oak does not cast a dense shadow, and therefore allows other trees or shrubs to grow in lower layer. By contrast, beech casts a dense shadow under which relatively few plants can grow (e.g. shade-tolerant seedlings of beech). As a result, while the presence of relatively small openings in the canopy cover, as those mapped here (75% smaller than 7 m^2) might have an influence on the growth and diversification of the understorey in Quercus and Mixed forest types, the same level of canopy openness is not sufficient to modify light availability under beech canopy cover. This is confirmed by the relatively low-density values of beech understorey.

The patch metrics correlated to the understorey parameters, in Mixed and Quercus forest types, are all shape metrics (except for the mean dbh in mixed forest). The density and development of the understorey in Mixed forest, namely, tend to increase as gap shape fits to an ellipse. A similar trend is observed in Quercus forest, where the mean dbh positively correlates with gap shape, when it fits to a rectangular geometry. On the other hand, the negative correlation between diversity of the understorey in Quercus forest and its covariate (standard deviation of Rectangular fit) has not a straightforward ecological interpretation.

It seems reasonable that the diversity and development of the understorey can be affected by the micro-porosity pattern of canopy cover, which light can shine through. The cumulative effect of differently shaped small gaps affects understorey development under forest canopies dominated by Turkey oak and mixtures between Turkey oak and beech. In fact, two differents gaps with the same extent can have different shape metrics. Our findings suggest that regular shapes (rectangular or elliptic) are influential for undestory density and diameter growth.

This is a relatively new finding in literature, as most authors focused their attention on relationships between gap size and understorey features. Popma and Bongers [83] for instance demonstrated that the growth and the morphology of seedling in a tropical rain forest depended on the size of gaps, likewise the dominance of understorey vegetation by shade tolerant species or shade intolerant ones [84].

4.3 Modeling living trees biodiversity through canopy gaps covariates

As for the understorey, strong correlations were found between canopy shape gaps metrics and density of micro-habitat bearing living trees and vertical species profile in Quercus and Mixed forest types.

The patch metric correlated to the density of micro-habitat bearing trees in canopies dominated by Turkey oak, are negatively related to the presence of gaps fitting into a rectangular shape (Sum_rect fit), whereas vertical diversification in species profile is negatively correlated with the variability of gap density (Sd_Density), which reflects variability from filament shape (low value) to high dense shape (square). In mixed forest stands, the density of micro-habitat bearing trees is negatively related to the variability of gaps length (CV_Lenght), while the mean height of the stand is positively correlated with the variability in gap shape asymmetry (Sd_Asym).

There might be different interpretations for these findings. Firstly, we could assume that the presence of canopy openings affects the growth in diameter and height of living trees. Schliemann and Bockheim [72] stipulated that after the opening of the canopy, the increased solar radiation allows plants to grow faster. Accordingly, the observed micro-porosity of canopy cover might favor sunlight penetration into the canopy layer(s), enabling conditions for species distribution along the

vertical profile. In addition, the increased exposure to weather conditions and biotic agents might influence micro-habitat differentiation along the trunk and branches (e.g. cavities and holes, injuries and wounds, trunk and crown breakage, epixilic species colonization). This idea was primarily developed by Runkle [85] who contended that in a tree fall gap, the microclimate changes associated to the gap formation extend to the bases of trees surrounding the canopy gap. Secondly, one might argue that micro-habitat bearing trees, which are frequently old large trees, create a structural diversity in the forest canopy because of their multiple dead tops, bole and top decays. This specific structure influences the canopy arrangement and creates, therefore, small canopy gaps with specific patch metrics that can be used as a footprint of habitat trees occurrence.

4.4 Comparison with other studies and implications

In the Mediterranean region characterized by complex environmental conditions and high seasonal variability of vegetation properties, UAV remote sensing offers advantages for capturing canopy parameters correlated with biodiversity metrics, in terms of costs and precision compared to alternative remote sensing technologies. A potential niche UAV fills – by providing covariates that combined with field-based forest inventory data – can be used in regression models for the spatial estimation of forest biodiversity variables over small forest areas. This study showed that canopy openness metrics can be used to predict by linear regression, in certain types of broadleaved deciduous forests, understorey features (density, development and diversity), vertical species profile and functional forest ecosystem attributes such as density of micro-habitat bearing trees, which are considered difficult to measure directly [86]. This latter result, is particularly interesting considering the recent attention given to the inventory of tree microhabitats [87].

The results obtained in this study are far from being random or happening by chance. The correlation was controlled using permutation tests [59] and all linear regression models satisfied linear regression assumptions. The confidence of the results was further bolstered by bootstrap resampling technique. To the best of our knowledge, this study is the first investigating the relationship between living trees parameters such as habitat trees and gap patch metrics from UAV RGB images.

Gap size distribution was roughly the same in the three forest types, with over 75% of gaps being smaller than 7 m^2, when gaps smaller than 2 m^2 are not considered. Strong relationships between this micro-porosity of the canopy layer and ecological phenomena beneath and inside the forest canopy were found only in two out of the three examined forest types. This finding suggests that variability in canopy cover composition and the size of field inventory plots, are to be taken into account when dealing with phenomena associated with spatial patterns of sunlight penetration into the canopy.

In this regard, the poor results of our study in beech dominated forest types, stemmed partially from the field inventory plot size, which might have been too small to capture significant relationships. Fagus forest is constituted with few big trees per plot. These horizontal and vertical structures make it impossible to observe a great variety of canopy gaps, in a plot of only 529 m^2. In their study, Getzin et al. [37] found relevant relationships in forest areas with beech as canopy dominant species, using plots almost twenty times larger than the plot size adopted in this study.

Furthermore, gap age is another important characteristic that could be taken into account to improve the quality of correlations. A newly opened gap has different biodiversity characteristics [1] and its effect on understorey and living trees would be minimal compared to an old gap of the same size and shape. Therefore, gap age can be used as another gap variable to be tested in future studies where forest canopy gaps are used as covariates of biodiversity-related variables of interest.

5. Conclusions

In conclusion, this research highlights that UAV remote sensing can potentially provide covariate surfaces of variables of interest for forest biodiversity monitoring, conventionally collected in forest inventory plots. By integrating the two sources of data, these variables can be mapped over small forest areas with satisfactory levels of accuracy, at a much higher spatial resolution than would

be possible by field-based forest inventory solely. From a statistical perspective, it matters little if the covariate that best correlates with the variable of interest is e.g. a gap shape or size metrics. Nonetheless, knowledge of the nature and sign of these correlations, can help to inform gap-based silvicultural approaches, aiming to favor the development and temporal continuity of these specific biodiversity components. This knowledge is crucial in the new silivicultural paradigm where managers adopt operations mimicking the nature [72].

Author Contributions: The five authors fully contributed in the research. MB and DG conducted the data analysis; DG and AB collected field data; FG, GC, DG and AB participated in UAV images collection and treatment. MB and FG wrote the document and AB discussed the results and their implications.

Funding: This research was supported by the EU LIFE program, in the framework of the project "FREShLIFE - Demonstrating Remote Sensing integration in sustainable forest management" (LIFE14 ENV/IT/000414). This work further benefited from the Erasmus Mundus MEDFOR (Mediterranean Forestry and Natural Resources Management) (520137-1-2011-1-PT-ERA MUNDUS-EMMC) fund.

Conflicts of Interest: The authors declare no conflict of interest.

Appendix A

Table 6. Summary description of patch metrics

Patch metric	Formula	Values range	Description
Border length (b_v)		[0, ∞)	Is basically the perimeter of the gap
Length (l_v)	$\sqrt{P_v \cdot \gamma_v}$	[0, ∞)	P_v is the total number of pixels contained in the patch v γ_v is the length-width ratio of an image object v
Length/Width (γ_v)	-	[0, ∞)	The length-to-width ratio of an image object
Width (w_v)	$\frac{P_v}{\gamma_v}$	[0, ∞)	The width of an image object is calculated using the length-to-width ratio
Asymmetry	-	[0,1]	The Asymmetry feature describes the relative length of an image object, compared to a regular polygon. An ellipse is approximated around a given image object, which can be expressed by the ratio of the lengths of its minor and the major axes. The feature value increases with this asymmetry.
Border Index	$\frac{b_v}{2 \bullet (l_v + w_v)}$	[1, ∞) 1=ideal	The Border Index feature describes how jagged an image object is; the more jagged, the higher its border index. This feature is similar to the Shape Index feature, but the Border Index feature uses a rectangular approximation instead of a square. The smallest rectangle enclosing the image object is created and the border index is calculated as the ratio between the border lengths of the image object and the smallest enclosing rectangle
Compactness	-	[0, ∞) 1=ideal	The Compactness feature describes how compact an image object is. It is similar to Border Index, but is based on area. However, the more compact an image object is, the smaller its border appears. The compactness of an image object is the product of the length and the width, divided by the number of pixels.
Density	-	[0, depending on shape of image object]	The Density feature describes the distribution in space of the pixels of an image object. In eCognition Developer 9.0 the most "dense" shape is a square; the more an object is shaped like a filament, the lower its density. The density is calculated by the number of pixels forming the image object

Peer-reviewed version available at Remote Sens. 2018, 10, 1397; doi:10.3390/rs10091397

Patch metric	Formula	Values range	Description
			divided by its approximated radius, based on the covariance matrix
Elliptic Fit	-	[0,1] ; 1 = complete fitting, 0 = <50% fit.	The Elliptic Fit feature describes how well an image object fits into an ellipse of similar size and proportions. While 0 indicates no fit, 1 indicates a perfect fit. The calculation is based on an ellipse with the same area as the selected image object. The proportions of the ellipse are equal to the length to the width of the image object. The area of the image object outside the ellipse is compared with the area inside the ellipse that is not filled by the image object
Radius of Largest Enclosed Ellipse ($\varepsilon_v^{\max}$)	-	[0, ∞)	The Radius of Largest Enclosed Ellipse feature describes how similar an image object is to an ellipse. The calculation uses an ellipse with the same area as the object and based on the covariance matrix. This ellipse is scaled down until it is totally enclosed by the image object. The ratio of the radius of this largest enclosed ellipse to the radius of the original ellipse is returned as a feature value.
Radius of Smallest Enclosing Ellipse ($\varepsilon_v^{\min}$)	-	[0, ∞)	The Radius of Smallest Enclosing Ellipse feature describes how much the shape of an image object is similar to an ellipse. The calculation is based on an ellipse with the same area as the image object and based on the covariance matrix. This ellipse is enlarged until it encloses the image object in total. The ratio of the radius of this smallest enclosing ellipse to the radius of the original ellipse is returned as a feature value.
Rectangular Fit	-	[0,1] ; where 1 is a perfect rectangle.	The Rectangular Fit feature describes how well an image object fits into a rectangle of similar size and proportions. While 0 indicates no fit, 1 indicates for a complete fitting image object. The calculation is based on a rectangle with the same area as the image object. The proportions of the rectangle are equal to the proportions of the length to width of the image object. The area of the image object outside the rectangle is compared with the area inside the rectangle.
Roundness	$\varepsilon_v^{\max} - \varepsilon_v^{\min}$	[0, ∞); 0 = ideal	The Roundness feature describes how similar an image object is to an ellipse. It is calculated by the difference of the enclosing ellipse and the enclosed ellipse.

Patch metric	Formula	Values range	Description
Shape Index	$b_v / 4\sqrt{A}$	[1,∞) ; 1 = ideal	The Shape index describes the smoothness of an image object border. The smoother the border of an image object is, the lower its shape index
Gap shape complexity index (GSCI)	$b_v / \sqrt{4\pi A}$	[1,∞) ; 1 = perfect circle	It is the ratio of a gap's perimeter to the perimeter of a circular gap of the same area
Patch fractal dimension (PFD)	$2 \cdot ln(b_v) / ln($	-	-
Fractal dimension (FD)	$2 \cdot ln(b_v / 4) / ln$	-	-
fractal dimension index (FDI)	$2 \cdot ln(b_v / \sqrt{4\pi}$	-	-

Appendix B. Correlations with understorey data

Table 7. Coefficient of correlations of Pearson and Spearman for some selected explicative and understorey dependent variables in Quercus forest

	N_PLANTS	N_SPECIES	I_SHANNON	I_PIELOU	MEAN_DBH	MEAN_HTOT	V_TOT	G_TOT
	Mdn_GSCI	Sd_rect.fit	Sd_rect.fit	Sd_Density	Avg_rect fit	Mdn_B. Index	Mdn_Asy	Avg_Asy
Threshold	1m²	2m²	2m²	1m²	1m²	2m²	1m²	1m²
Pearson	0.73	-0.66	-0.75	-0.64	0.79	-0.58	-0.64	-0.57
Spearman	0.70	-0.73	-0.88	-0.68	0.75	-0.67	-0.57	-0.55

Table 8. Coefficient of correlation of Pearson and Spearman for some selected explicative and dependent variables in mixed forest

	N_PLANTS	N_SPECIES	I_SHANNON	I_PIELOU	MEAN_DBH	MEAN_HTOT	G_TOT	V_TOT
	Avg_Round.	Mdn_RSE	Mdn_RSE	avg_RLE	Sum_width	Avg_Asym.	Sd_Asym.	Avg_Comp.
Threshold	2m²	1m²	1m²	2 m²	2m²	2m²	2m²	2m²
Pearson	-0.81	0.73	0.69	0.71	-0.78	0.94	0.72	-0.67
Spearman	-0.83	0.70	0.70	0.75	-0.70	0.92	0.72	-0.77

Table 9. Coefficient of correlation of Pearson and Spearman for some selected explicative and dependent variables in Fagus forest

	N_SPECIES	I_SHANNON	I_PIELOU	MEAN_HTOT
	Cv_Round	Sd_Round	Mdn_PFD	cv_Lenght
Threshold	1 m²	1 m²	1 m²	2 m²
Pearson	-0.43	0.50	0.74	0.52
Spearman	-0.45	0.56	0.87	0.57

Appendix C. Correlations with living trees data

Table 10. Coefficient of correlations of Pearson and Spearman for some selected explicative and living trees dependent variables in Quercus forest

	N_SPECIES	I_SHANNON	I_MARGALEF	I_PRETZSCH	MEAN_DBH	MEAN_HTOT	HAB	%HAB
	Sd_rect_fit	Cv_Density	Sd_rect_fit	Sd_Density	Sum_rect.fit	Mdn_rect.fit	Sum_rect.fit	Sum_RLE
Threshold	2m²	2m²	2m²	2m²	1m²	1m²	2m²	2m²
Pearson	-0.68	-0.64	-0.71	-0.87	0.61	0.59	-0.79	-0.71

Spearman	-0.72	-0.61	-0.74	-0.90	0.70	0.56	-0.70	-0.64

Table 11. Coefficient of correlations of Pearson and Spearman for some selected explicative and living trees dependent variables in Mixed forest

	MEAN_DBH	MEAN_HTOT	HAB	%HAB
	Avg_Round.	Sd_Asym.	Cv_Length	Avg_RSE
Threshold	2m²	1m²	2m²	1m²
Pearson	0.74	-0.84	-0.90	-0.83
Spearman	0.82	-0.95	-0.92	-0.92

Table 12. Coefficient of correlations of Pearson and Spearman for some selected explicative and living trees dependent variables in Fagus forest

2m	HAB	%HAB
	cv_PFD	Avg_RSE
Pearson	0.43	-0.38
Spearman	0.50	-0.39

References

1. Muscolo, A.; Bagnato, S.; Sidari, M.; Mercurio, R. A review of the roles of forest canopy gaps. *J. For. Res.* **2014**, *25*, 725–736, doi:10.1007/s11676-014-0521-7.
2. Karsten, R. J.; Jovanovic, M.; Meilby, H.; Perales, E.; Reynel, C. Regeneration in canopy gaps of tierra-firme forest in the Peruvian Amazon: Comparing reduced impact logging and natural, unmanaged forests. *For. Ecol. Manage.* **2013**, *310*, 663–671, doi:10.1016/j.foreco.2013.09.006.
3. Stan, A. B.; Daniels, L. D. Growth releases across a natural canopy gap-forest gradient in old-growth forests. *For. Ecol. Manage.* **2014**, *313*, 98–103, doi:10.1016/j.foreco.2013.11.004.
4. Feldmann, E.; Drößler, L.; Hauck, M.; Kucbel, S.; Pichler, V.; Leuschner, C. Canopy gap dynamics and tree understory release in a virgin beech forest, Slovakian Carpathians. *For. Ecol. Manage.* **2018**, *415–416*, 38–46, doi:10.1016/j.foreco.2018.02.022.
5. Amir, A. A. Canopy gaps and the natural regeneration of Matang mangroves. *For. Ecol. Manage.* **2012**, *269*, 60–67, doi:10.1016/j.foreco.2011.12.040.
6. Muscolo, A.; Settineri, G.; Bagnato, S.; Mercurio, R.; Sidari, M. Use of canopy gap openings to restore coniferous stands in Mediterranean environment. *iForest* **2017**, *10*, 322, doi:10.3832/IFOR1983-009.
7. Čater, M.; Diaci, J.; Roženbergar, D. Gap size and position influence variable response of Fagus sylvatica L. and Abies alba Mill. *For. Ecol. Manage.* **2014**, *325*, 128–135, doi:10.1016/j.foreco.2014.04.001.
8. Getzin, S.; Nuske, R. S.; Wiegand, K. Using unmanned aerial vehicles (UAV) to quantify spatial gap patterns in forests. *Remote Sens.* **2014**, *6*, 6988–7004, doi:10.3390/rs6086988.
9. Nagendra, H. Using remote sensing to assess biodiversity. *Int. J. Remote Sens.* **2001**, *22*, 2377–2400, doi:10.1080/01431160117096.
10. Tang, L.; Shao, G. Drone remote sensing for forestry research and practices. *J. For. Res.* **2015**, *26*, 791–797, doi:10.1007/s11676-015-0088-y.
11. Giannetti, F.; Chirici, G.; Gobakken, T.; Naesset, E.; Travaglini, D.; Puliti, S. A new set of DTM-independent metrics for forest growing stock prediction using UAV photogrammetric data. *Remote Sens. Environ.*

12. Torresan, C.; Berton, A.; Carotenuto, F.; Di Gennaro, S. F.; Gioli, B.; Matese, A.; Miglietta, F.; Vagnoli, C.; Zaldei, A.; Wallace, L. Forestry applications of UAVs in Europe: a review. *Int. J. Remote Sens.* **2017**, *38*, 2427–2447, doi:10.1080/01431161.2016.1252477.
13. Puliti, S.; Olerka, H.; Gobakken, T.; Næsset, E. Inventory of Small Forest Areas Using an Unmanned Aerial System. *Remote Sens.* **2015**, *7*, 9632–9654, doi:10.3390/rs70809632.
14. Dandois, J. P.; Ellis, E. C. High spatial resolution three-dimensional mapping of vegetation spectral dynamics using computer vision. *Remote Sens. Environ.* **2013**, *136*, 259–276, doi:10.1016/j.rse.2013.04.005.
15. Fardusi, M. J.; Chianucci, F.; Barbati, A. Concept to practices of geospatial information tools to assist forest management & planning under precision forestry framework: A review. *Ann. Silvic. Res.* **2017**, *41*, 3–14, doi:10.12899/asr-1354.
16. Remondino, F.; Spera, M. G.; Nocerino, E.; Menna, F.; Nex, F. State of the art in high density image matching. *Photogramm. Rec.* **2014**, *29*, 144–166, doi:10.1111/phor.12063.
17. Zahawi, R. A.; Dandois, J. P.; Holl, K. D.; Nadwodny, D.; Reid, J. L.; Ellis, E. C. Using lightweight unmanned aerial vehicles to monitor tropical forest recovery. *Biol. Conserv.* **2015**, *186*, 287–295, doi:10.1016/j.biocon.2015.03.031.
18. Alonzo, M.; Andersen, H.-E.; Morton, D.; Cook, B. Quantifying Boreal Forest Structure and Composition Using UAV Structure from Motion. *Forests* **2018**, *9*, 119, doi:10.3390/f9030119.
19. Messinger, M.; Asner, G. P.; Silman, M. Rapid assessments of amazon forest structure and biomass using small unmanned aerial systems. *Remote Sens.* **2016**, *8*, 1–15, doi:10.3390/rs8080615.
20. Chianucci, F.; Disperati, L.; Guzzi, D.; Bianchini, D.; Nardino, V.; Lastri, C.; Rindinella, A.; Corona, P. Estimation of canopy attributes in beech forests using true colour digital images from a small fixed-wing UAV. *Int. J. Appl. Earth Obs. Geoinf.* **2016**, *47*, 60–68, doi:10.1016/j.jag.2015.12.005.
21. Lisein, J.; Michez, A.; Claessens, H.; Lejeune, P. Discrimination of deciduous tree species from time series of unmanned aerial system imagery. *PLoS One* **2015**, *10*, 1–20, doi:10.1371/journal.pone.0141006.
22. Lehmann, J. R. K.; Nieberding, F.; Prinz, T.; Knoth, C. Analysis of unmanned aerial system-based CIR images in forestry-a new perspective to monitor pest infestation levels. *Forests* **2015**, *6*, 594–612, doi:10.3390/f6030594.
23. Hall, R. J.; Castilla, G.; White, J. C.; Cooke, B. J.; Skakun, R. S. Remote sensing of forest pest damage: a review and lessons learned from a Canadian perspective. *Can. Entomol.* **2016**, *148*, s296–s356, doi:10.4039/tce.2016.11.
24. Michez, A.; Piégay, H.; Lisein, J.; Claessens, H.; Lejeune, P. Classification of riparian forest species and health condition using multi-temporal and hyperspatial imagery from unmanned aerial system. *Environ. Monit. Assess.* **2016**, *188*, 146, doi:10.1007/s10661-015-4996-2.
25. Myers, D.; Ross, C. M.; Liu, B. A Review of Unmanned Aircraft System (UAS) Applications for Agriculture. *2015 ASABE Int. Meet.* **2015**, 1, doi:10.13031/aim.20152189593.
26. Lisein, J.; Linchant, J.; Lejeune, P.; Bouche, P.; Vermeulen, C. Aerial surveys using an Unmanned Aerial System (UAS): comparison of different methods for estimating the surface area of sampling strips. *Trop. Conserv. Sci.* **2013**, *6*, 506–520.
27. Colomina, I.; Molina, P. Unmanned aerial systems for photogrammetry and remote sensing: A review. *J. Photogramm. Remote Sens.* **2014**, *7*, 9632–9654, doi:10.1016/j.isprsjprs.2014.02.013.
28. Sandbrook, C. The social implications of using drones for biodiversity conservation. *Ambio* **2015**, *44*, 636–647, doi:10.1007/s13280-015-0714-0.
29. Zhang, J.; Hu, J.; Lian, J.; Fan, Z.; Ouyang, X.; Ye, W. Seeing the forest from drones: Testing the potential

694 of lightweight drones as a tool for long-term forest monitoring. *Biol. Conserv.* **2016**, *198*, 60–69,
695 doi:10.1016/j.biocon.2016.03.027.
696 30. Anderson, K.; Gaston, K. J. Lightweight unmanned aerial vehicles will revolutionize spatial ecology.
697 *Front. Ecol. Environ.* **2013**, *11*, 138–146, doi:10.1890/120150.
698 31. Paneque-Gálvez, J.; McCall, M. K.; Napoletano, B. M.; Wich, S. A.; Koh, L. P. Small drones for
699 community-based forest monitoring: An assessment of their feasibility and potential in tropical areas.
700 *Forests* **2014**, *5*, 1481–1507, doi:10.3390/f5061481.
701 32. Turner, D.; Lucieer, A.; Watson, C. An automated technique for generating georectified mosaics from
702 ultra-high resolution Unmanned Aerial Vehicle (UAV) imagery, based on Structure from Motion (SFM)
703 point clouds. *Remote Sens.* **2012**, *4*, 1392–1410, doi:10.3390/rs4051392.
704 33. Zielewska-Büttner, K.; Adler, P.; Ehmann, M.; Braunisch, V. Automated Detection of Forest Gaps in
705 Spruce Dominated Stands using Canopy Height Models Derived from Stereo Aerial Imagery. *Remote*
706 *Sens.* **2016**, *8*, 1–21, doi:10.3390/rs8030175.
707 34. Betts, H. D.; Brown, L. J.; Stewart, G. H. Forest canopy gap detection and characterisation by the use of
708 high- resolution Digital Elevation Models. *N. Z. J. Ecol.* **2005**, *29*, 95–103.
709 35. Seidel, D.; Ammer, C.; Puettmann, K. Describing forest canopy gaps efficiently, accurately, and
710 objectively: New prospects through the use of terrestrial laser scanning. *Agric. For. Meteorol.* **2015**, *213*,
711 23–32, doi:10.1016/j.agrformet.2015.06.006.
712 36. Bonnet, S.; Gaulton, R.; Lehaire, F.; Lejeune, P. Canopy gap mapping from airborne laser scanning: An
713 assessment of the positional and geometrical accuracy. *Remote Sens.* **2015**, *7*, 11267–11294,
714 doi:10.3390/rs70911267.
715 37. Getzin, S.; Wiegand, K.; Schöning, I. Assessing biodiversity in forests using very high-resolution images
716 and unmanned aerial vehicles. *Methods Ecol. Evol.* **2012**, *3*, 397–404, doi:10.1111/j.2041-210X.2011.00158.x.
717 38. Turner, D.; Lucieer, A.; Wallace, L. Direct georeferencing of ultrahigh-resolution UAV imagery. *IEEE*
718 *Trans. Geosci. Remote Sens.* **2014**, *52*, 2738–2745, doi:10.1109/TGRS.2013.2265295.
719 39. Czapski, P.; Kacprzak, M.; Kotlarz, J.; Mrowiec, K.; Kubiak, K.; Tkaczyk, M. Preliminary analysis of the
720 forest health state based on multispectral images acquired by Unmanned Aerial Vehicle. *Folia For. Pol.*
721 **2015**, *57*, 138–144, doi:10.1515/ffp-2015-0014.
722 40. Scoppola, A.; Caporali, C. Mesophilous woods with Fagus sylvatica L. of Northern Latium (Tyrrenian
723 Central Italy): synecology and syntaxonomy. *Plant Biosyst.* **1998**, *132*, 151–168.
724 41. Winter, S.; Möller, G. C. Microhabitats in lowland beech forests as monitoring tool for nature
725 conservation. *For. Ecol. Manage.* **2008**, *255*, 1251–1261, doi:10.1016/j.foreco.2007.10.029.
726 42. Assmann, E. *The principles of forest yield study.*; Pergamon Press. Oxford, 1970;
727 43. Shannon, C. A mathematical theory of communication. *Bell Syst. Tech. J.* **1948**, *27*, 379–423.
728 44. Pielou, E. C. *Ecological Diversity*; New York, 1975;
729 45. Clifford, H. T.; Stephenson, W. *An introduction to numerical classification*; Academic Press, 1975; ISBN
730 9780121767501.
731 46. Agisoft LLC Agisoft PhotoScan User Manual. Available online http://www.agisoft.com/pdf/photoscan-
732 pro_1_3_en.pdf (accessed on 11 April 2017). **2017**.
733 47. Kachamba, D.; Ørka, O. H.; Gobakken, T.; Eid, T.; Mwase, W. Biomass Estimation Using 3D Data from
734 Unmanned Aerial Vehicle Imagery in a Tropical Woodland. *Remote Sens.* **2016**, *8*, 968,
735 doi:10.3390/RS8110968.
736 48. Lisein, J.; Pierrot-Deseilligny, M.; Bonnet, S.; Lejeune, P. A photogrammetric workflow for the creation

of a forest canopy height model from small unmanned aerial system imagery. *Forests* **2013**, *4*, 922–944, doi:10.3390/f4040922.

49. Puliti, S.; Gobakken, T.; Ørka, H. O.; Næsset, E. Assessing 3D point clouds from aerial photographs for species-specific forest inventories. *Scand. J. For. Res.* **2017**, *32:1*, 68–79, doi:10.1080/02827581.2016.1186727.
50. Wallace, L.; Lucieer, A.; Malenovsky, Z.; Turner, D.; Vopenka, P. Assessment of forest structure using two UAV techniques: A comparison of airborne laser scanning and structure from motion (SfM) point clouds. *Forests* **2016**, *7*, 1–16, doi:10.3390/f7030062.
51. Dezso, B.; Fekete, I.; Gera, D.; Giachetta, R.; László, I.; Benczúr, A.; Dezs″, B.; Fekete, I.; Gera, D.; Giachetta, R.; László, I. Object-based image analysis in remote sensing applications using various segmentation techniques. *Ann. Univ. Sci. Budapest., Sect. Comp* **2012**, *37*, 103–120.
52. Trimble *Segmentation Algorithms*; 9.01.; Trimble Germany GmbH, Arnulfstrasse 126, D-80636 Munich, Germany, 2014;
53. Koukoulas, S.; Blackburn, G. A. Quantifying the spatial properties of forest canopy gaps using LiDAR imagery and GIS. *Int. J. Remote Sens.* **2004**, *25*, 3049–3072, doi:10.1080/01431160310001657786.
54. Moser, D.; Zechmeister, H. G.; Plutzar, C.; Sauberer, N.; Wrbka, T.; Grabherr, G. Landscape patch shape complexity as an effective measure for plant species richness in rural landscapes. *Landsc. Ecol.* **2002**, *17*, 657–669, doi:10.1023/A:1021513729205.
55. Eysenrode, D. S.; Bogaert, J.; Hecke, P. Van; Impens, I. Influence of tree-fall orientation on canopy gap shape in an Ecuadorian rain forest. *J. Trop. Ecol.* **1998**, *14*, 865–869, doi:10.1017/S0266467498000625.
56. Saura, S.; Carballal, P. Discrimination of native and exotic forest patterns through shape irregularity indices: An analysis in the landscapes of Galicia, Spain. *Landsc. Ecol.* **2004**, *19*, 647–662.
57. Busing, R. T. Canopy cover and tree regeneration in old-growth cove forests of the Appalachian Mountains. *Vegetatio* **1994**, *115*, 19–27.
58. Main-Knorn, M.; Moisen, G. G.; Healey, S. P.; Keeton, W. S.; Freeman, E. A.; Hostert, P. Evaluating the remote sensing and inventory-based estimation of biomass in the western carpathians. *Remote Sens.* **2011**, *3*, 1427–1446, doi:10.3390/rs3071427.
59. Legendre, P.; Legendre, L. *Development in Environmental Modelling: Numerical Ecology*; 2nd Englis.; Elsevier B.V.: Amsterdam, 1983;
60. James, G.; Witen, D.; Hastie, T.; Tibshirani, R. *An Introduction to Statistical Learning with Applications in R*; Castilla, G., Fienberg, S., Olkin, I., Eds.; Springer.; Springer New York Heidelberg Dordrecht London, 2017; Vol. 64; ISBN 9780387781884.
61. Hauke, J.; Kossowski, T. Comparison of values of Pearson's and Spearman's correlation coefficients on the same sets of data. *Quaest. Geogr.* **2011**, *30*, 87–93, doi:10.2478/v10117-011-0021-1.
62. Møller, A. P.; Jennions, M. D. How much variance can be explained by ecologists and evolutionary biologists? *Oecologia* **2002**, *132*, 492–500, doi:10.1007/s00442-002-0952-2.
63. Mura, M.; McRoberts, R. E.; Chirici, G.; Marchetti, M. Statistical inference for forest structural diversity indices using airborne laser scanning data and the k-Nearest Neighbors technique. *Remote Sens. Environ.* **2016**, *186*, 678–686, doi:10.1016/j.rse.2016.09.010.
64. Lyons, M. B.; Keith, D. A.; Phinn, S. R.; Mason, T. J.; Elith, J. A comparison of resampling methods for remote sensing classification and accuracy assessment. *Remote Sens. Environ.* **2018**, *208*, 145–153, doi:10.1016/j.rse.2018.02.026.
65. McRoberts, R. E.; Magnussen, S.; Tomppo, E. O.; Chirici, G. Parametric, bootstrap, and jackknife variance estimators for the k-Nearest Neighbors technique with illustrations using forest inventory and satellite

image data. *Remote Sens. Environ.* **2011**, *115*, 3165–3174, doi:10.1016/j.rse.2011.07.002.

66. Rao, J. N. K. Jackknife and bootstrap methods for small area estimation. Proceedings of the survey research methods section. In *American Statistical Association*; 2007.
67. Efron, B.; Tibshirani, R. Improvements on cross-validation: The .632 plus bootstrap method. *J. Am. Stat. Assoc.* **1997**, *92*, 548, doi:10.1080/01621459.1997.10474007.
68. Boyd, D. S.; Hill, R. A.; Hopkinson, C.; Baker, T. R. Landscape-scale forest disturbance regimes in southern Peruvian. *Ecol. Appl.* **2013**, *23*, 1588–1602.
69. Senécal, J. F.; Doyon, F.; Messier, C. Tree death not resulting in gap creation: An investigation of canopy dynamics of northern temperate deciduous forests. *Remote Sens.* **2018**, *10*, doi:10.3390/rs10010121.
70. Senécal, J. F.; Doyon, F.; Messier, C. Management implications of varying gap detection height thresholds and other canopy dynamics processes in temperate deciduous forests. *For. Ecol. Manage.* **2018**, *410*, 84–94, doi:10.1016/j.foreco.2017.12.029.
71. Vepakomma, U.; St-Onge, B.; Kneeshaw, D. Spatially explicit characterization of boreal forest gap dynamics using multi-temporal lidar data. *Remote Sens. Environ.* **2008**, *112*, 2326–2340, doi:10.1016/j.rse.2007.10.001.
72. Schliemann, S. A.; Bockheim, J. G. Methods for studying treefall gaps: A review. *For. Ecol. Manage.* **2011**, *261*, 1143–1151, doi:10.1016/j.foreco.2011.01.011.
73. Hobi, M. L.; Ginzler, C.; Commarmot, B.; Bugmann, H. Gap pattern of the largest primeval beech forest of Europe revealed by remote sensing. *Ecosphere* **2015**, *6*, art76, doi:10.1890/ES14-00390.1.
74. Brokaw, N. V. L. The Definition of Treefall Gap and Its Effect on Measures of Forest Dynamics. *Biotropica* **1982**, *14*, 158, doi:10.2307/2387750.
75. White, J. C.; Tompalski, P.; Coops, N. C.; Wulder, M. A. Comparison of airborne laser scanning and digital stereo imagery for characterizing forest canopy gaps in coastal temperate rainforests. *Remote Sens. Environ.* **2018**, *208*, 1–14, doi:10.1016/j.rse.2018.02.002.
76. Kane, V. R.; Gersonde, R. F.; Lutz, J. A.; McGaughey, R. J.; Bakker, J. D.; Franklin, J. F. Patch dynamics and the development of structural and spatial heterogeneity in Pacific Northwest forests. *Can. J. For. Res.* **2011**, *41*, 2276–2291, doi:10.1139/x11-128.
77. Asner, G. P.; Kellner, J. R.; Kennedy-Bowdoin, T.; Knapp, D. E.; Anderson, C.; Martin, R. E. Forest Canopy Gap Distributions in the Southern Peruvian Amazon. *PLoS One* **2013**, *8*, doi:10.1371/journal.pone.0060875.
78. Zielewska-Büttner, K.; Adler, P.; Petersen, M.; Braunisch, V. Parameters Influencing Forest Gap Detection Using Canopy Height Models Derived From Stereo Aerial Imagery. *Publ. der DGPF* **2016**, *25*, 405–416.
79. Perroy, R. L.; Sullivan, T.; Stephenson, N. Assessing the impacts of canopy openness and flight parameters on detecting a sub-canopy tropical invasive plant using a small unmanned aerial system. *ISPRS J. Photogramm. Remote Sens.* **2017**, *125*, 174–183, doi:10.1016/j.isprsjprs.2017.01.018.
80. Lombard, L.; Ismail, R.; Poona, N. Modelling forest canopy gaps using LiDAR-derived variables. *Geocarto Int.* **2017**, *6049*, 1–15, doi:10.1080/10106049.2017.1377775.
81. Ma, L.; Zheng, G.; Wang, X.; Li, S.; Lin, Y.; Ju, W. Retrieving forest canopy clumping index using terrestrial laser scanning data. *Remote Sens. Environ.* **2018**, *210*, 452–472, doi:10.1016/j.rse.2018.03.034.
82. Barbati, A.; Chirici, G.; Corona, P.; Montaghi, A.; Travaglini, D. Area-based assessment of forest standing volume by field measurements and airborne laser scanner data. *Int. J. Remote Sens.* **2009**, *30*, 5177–5194, doi:10.1080/01431160903023017.

83. Popma, J.; Bongers, F. The effect of canopy gaps on growth and morphology of seedlings of rain forest species. *Oecologia* **1988**, *75*, 625–632, doi:10.1007/BF00776429.

84. Garbarino, M.; Borgogno Mondino, E.; Lingua, E.; Nagel, T. A.; Dukic, V.; Govedar, Z.; Motta, R. Gap disturbances and regeneration patterns in a Bosnian old-growth forest: a multispectral remote sensing and ground-based approach. *Ann. For. Sci.* **2012**, *69*, 617–625, doi:10.1007/s13595-011-0177-9.

85. Runkle, J. R. Patterns of Disturbance in Some Old-Growth Mesic Forests of Eastern North America. *Ecology* **1982**, *63*, 1533–1546, doi:10.2307/1938878.

86. Franklin, J. F.; Spies, T. A.; Pelt, R. Van; Carey, A. B.; Thornburgh, D. A.; Berg, D. R.; Lindenmayer, D. B.; Harmon, M. E.; Keeton, W. S.; Shaw, D. C.; Bible, K.; Chen, J. Disturbances and structural development of natural forest ecosystems with silvicultural implications, using Douglas-fir forests as an example. *For. Ecol. Manage.* **2002**, *155*, 399–423, doi:10.1016/S0378-1127(01)00575-8.

87. Larrieu, L.; Paillet, Y.; Winter, S.; Bütler, R.; Kraus, D.; Krumm, F.; Lachat, T.; Michel, A. K.; Regnery, B.; Vandekerkhove, K. Tree related microhabitats in temperate and Mediterranean European forests: A hierarchical typology for inventory standardization. *Ecol. Indic.* **2018**, *84*, 194–207, doi:10.1016/j.ecolind.2017.08.051.